Supporting Information

Intramolecular C–H and C–F Bond Oxygenation Mediated by a Putative Terminal Oxo Species in Tetranuclear Iron Complexes

Graham de Ruiter, Niklas B. Thompson, Michael K. Takase, and Theodor Agapie*

Division of Chemistry and Chemical Engineering, California Institute of Technology, Pasadena, California 91125, United States. Email: agapie@caltech.edu

Table of Contents

General Considerations.

All reactions were performed at room temperature in an N_2-filled M. Braun Glovebox or by using standard Schlenk techniques unless otherwise specified. Glassware was oven dried at 140° C for at least 2h prior to use, and allowed to cool under vacuum. All reagents were used as received unless otherwise stated. Iodosobenzene (PhIO), 2,6-difluorophenylpyrazole, 6-methoxy-2-fluoroacetophenone, and $[LFe_3(PhPz_3)OFe][OTf]_2$ (**1**) were synthesized according to published procedures.[1-4] *Caution! Iodosobenzene is potentially explosive and should be used only in small quantities.* Phenyl-*1H*-pyrazole, 3-(2-hydroxyphenyl)-*1H*-pyrazole, 6-methoxy-2-fluorobenzaldehyde, 2,6-difluoroacetophenone, $Na(N(SiMe_3)_2)$, and AgOTf, were purchased from Sigma Aldrich, Oakwood Chemicals and Strem Chemicals. All commercially available pyrazoles were sublimed before use. Anhydrous tetrahydrofuran (THF) was purchased from Aldrich in 18 L Pure-Pac^{TM} containers. Anhydrous CH_2Cl_2, diethyl ether, hexane and THF were purified by sparging with nitrogen for 15 minutes and then passing under nitrogen pressure through a column of activated A2 alumina. Anhydrous 1,2-dimethoxyethane (DME) was dried over sodium/benzophenone and vacuum-transferred onto molecular sieves. The ^1H, and $^{13}C\{^1H\}$ NMR spectra were recorded at 400.13, and 100.62 MHz on a Bruker Ascend^{TM} 400 MHz spectrometer equipped with prodigy cryoprobe, or at 300.13, 282.36 (^{19}F), and 75.47 MHz, respectively, on a Varian 300 MHz spectrometer. All chemical shifts (δ) are reported in ppm, and coupling constants (*J*) are in Hz. The ^1H and $^{13}C\{^1H\}$ NMR spectra were referenced using residual solvent peaks in the deuterated solvent. The ^{19}F chemical shifts are reported relative to the internal lock signal. Deuterated solvents (CD_2Cl_2 and CD_3CN) were purchased from Cambridge Isotope Laboratories, dried over calcium hydride, degassed by three freeze-pump-thaw cycles and vacuum-transferred prior to use. The UV-vis spectra were recorded on a Varian Cary Bio 50 spectrophotometer. Fast atom bombardment-mass spectrometry (FAB-MS) analysis was performed with a JEOL JMS-600H high resolution mass spectrometer. Gas chromatography-mass spectrometry (GC-MS) analysis was performed upon filtering the sample through a plug of alumina gel. Elemental analyses were performed by Midwest Microlab, IN, Robertson Microlit Laboratories, NJ, or at Caltech.

Physical Methods.

Mössbauer measurements. Zero-field ^{57}Fe Mössbauer spectra were recorded at 80 K in the constant acceleration mode on a spectrometer from See Co (Edina, MN) equipped with an SVT-

400 cryostat (Janis, Wilmington, WA). The quoted isomer shifts are relative to the centroid of the spectrum of a α-Fe foil at room temperature. Samples were prepared by grinding polycrystalline material (20 mg) into a fine powder and pressed into a homogeneous pellet with boron nitride in a cup fitted with a screw cap. The data were fitted to Lorentzian lineshapes using the program WMOSS (www.wmoss.org). For a detailed fitting procedure see page S37.

X-ray crystallography. For compounds **2**, **3**, **5**, **7**–**8**, low-temperature (100 K) diffraction data (ϕ-and ω-scans) were collected on a Bruker AXS D8 VENTURE KAPPA diffractometer coupled to a PHOTON 100 CMOS detector with Mo Kα radiation (λ = 0.71073 Å) or with Cu Kα (λ = 1.54178 Å). For compound **5**, low-temperature (100 K) diffraction data (ϕ-and ω-scans) were collected on a Bruker AXS KAPPA APEX II diffractometer coupled to an APEX II CCD detector with graphite monochromated Mo Kα radiation (λ = 0.71073 Å). All diffractometer manipulations, including data collection, integration, and scaling were carried out using the Bruker APEXII software.[5] Absorption corrections were applied using SADABS.[6] Structures were solved by direct methods using SHELXS[7] and refined against F^2 on all data by full-matrix least squares with SHELXL-2014 using established refinement techniques. All non-hydrogen atoms were refined anisotropically. All hydrogen atoms were included into the model at geometrically calculated positions and refined using a riding model. The isotropic displacement parameters of all hydrogen atoms were fixed to 1.2 times the U value of the atoms they are linked to (1.5 times for methyl groups). All disordered atoms were refined with the help of similarity restraints on the 1,2- and 1,3-distances and displacement parameters as well as enhanced rigid bond restraints for anisotropic displacement parameters. Due to the size of compounds (**2**, **3**, **5**, and **7**–**8**), most crystals included solvent accessible voids, which tended to contain disordered solvent. In most cases, this disorder could be modeled satisfactorily Furthermore, the long-range order of these crystals and amount of high angle data was in some cases not ideal, due to desolvation of the crystals and/or solvent disorder. These disordered solvent molecules were largely responsible for the alerts generated by the checkCIF protocol. Although several attempts were made to crystallize compound **8**, we were not able to obtain a crystal structure suitable for analysis of bond distances and angles. The structure contained within the manuscript and supporting information is only for structural identification only.

Synthetic Procedures

1-(2-fluoro-6-methoxyphenyl)ethan-1-ol. In the glovebox, to a thawing solution of 2-fluoro-6-methoxybenzaldehyde (2.5 g; 18.1 mmol) in diethyl ether (25 mL) was added MeMgBr (3.0 M in diethyl ether; 12 mL, 36.0 mmol). The resulting grey suspension was stirred for ca. 24 h. Next, the suspension was cooled, outside of the glovebox, to 0° C and carefully quenched with 3.0 M hydrochloric acid. Ethyl acetate (25 mL) was added and the aqueous phase extracted with ethyl acetate (3 × 25 mL). The organic fractions were pooled together, washed with brine, and dried over $MgSO_4$. The volatiles were removed under reduced pressure to yield 1-(2-fluoro-6-methoxyphenyl)ethan-1-ol as a colorless oil (2.55 g; 83%). ^{1}H NMR (400 MHz, $CDCl_3$) δ 7.19 (td, *J* = 8.3, 6.5 Hz, 1H; *p*-Ar*H*), 6.70 (td, *J* = 8.5, 1.2 Hz, 2H; *m*-Ar*H*), 5.25 (dq, *J* = 10.9, 6.7 Hz, 1H; C*H*CH_3), 3.90 (s, 3H; OCH_3), 3.37 (dd, *J* = 10.9, 1.2 Hz, 1H; O*H*), 1.58 (d, *J* = 6.7 Hz, 3H; CHCH_3). ^{13}C NMR (101 MHz, $CDCl_3$) δ 160.14 (d, *J* = 243.9 Hz; *C*-F), 158.30 (d, *J* = 8.0 Hz; *C*OMe), 128.50 (d, *J* = 11.0 Hz; *p*-Ar*C*), 120.33 (d, *J* = 16.5 Hz; *i*-Ar*C*), 108.60 (d, *J* = 23.6 Hz; *m*-Ar*C*), 106.77 (d, *J* = 2.9 Hz; *m*-Ar*C*), 63.47 (d, *J* = 5.8 Hz; *C*H), 55.89 (s; OCH_3), 23.69 (s; *C*H_3). ^{19}F NMR (282 MHz, $CDCl_3$) δ -118.15 (dd, *J* = 9.9, 6.6 Hz).

2-fluoro-6-methoxyacetophenone. To a solution of 1-(2-fluoro-6-methoxyphenyl)ethan-1-ol (2.55 g; 15 mmol) in DMF (30 mL) was added pyridinium dichromate (8.80 g; 23.5 mmol). The solution was stirred for ca. 24 h, where after H_2O (75 mL) was added. The resulting mixture was extracted with ethyl acetate (3 × 50 mL). The organic fractions were pooled together, washed with brine, and dried over $MgSO_4$. The volatiles were removed under reduced pressure to yield a crude yellow oil. The crude oil was purified by column chromatography (silica; 10:90 (v/v) ethyl acetate/hexane) to yield 2-fluoro-6-methoxyacetophenone as a colorless oil. Yield. 2.17 g (86%). ^{1}H NMR (400 MHz, $CDCl_3$) δ 7.33 (td, *J* = 8.4, 6.6 Hz, 1H; *p*-Ar*H*), 6.77 – 6.69 (m, 2H; *m*-Ar*H*), 3.87 (s, 3H; OCH_3), 2.56 (d, *J* = 1.2 Hz, 3H; CCH_3). ^{13}C NMR (101 MHz, $CDCl_3$) δ 198.85 (s; *C*O), 159.65 (d, *J* = 249.0 Hz; *C*-F), 157.62 (d, *J* = 7.7 Hz; *C*OMe), 131.52 (d, *J* = 10.6 Hz; *p*-Ar*C*), 119.39 (d, *J* = 19.0 Hz; *i*-Ar*C*), 108.39 (d, *J* = 22.3 Hz; *m*-Ar*C*), 106.87 (d, *J* = 3.0 Hz; *m*-Ar*C*), 56.16 (s; OCH_3), 32.43 (d, *J* = 1.4 Hz; CCH_3). ^{19}F NMR (282 MHz, $CDCl_3$) δ -115.63 – -115.72 (m).

3-(2-fluoro-6-methoxyphenyl)-1*H*-pyrazole. Under N_2, a Schlenk-tube was charged with 2-fluoro-6-methoxyacetophenone (2.17 g; 12.8 mmol) and *N,N*-dimethylformamide dimethylacetal (1.79 g; 15.0 mmol). The tube was sealed and heated at 110° C for ca. 16 h.

Next, the volatiles were removed under reduced pressure to yield an orange oil (1-(2-fluoro-6-methoxyphenyl)-3-(dimethylamino)-prop-2-en-1-one). The crude oil was used without further purification and dissolved in ethanol (20.0 mL). To the solution was added hydrazine monohydrate (1.0 mL; 20.6 mmol) and acetic acid (1.1 mL; 19.1 mmol) at 0° C. The mixture was stirred for 3 h. at 70° C, during which the color changed from orange to yellow. Hereafter, the ethanol was removed under reduced pressure and the remaining solid was dissolved in ethyl acetate (20 mL). To the solution was added sat. sodium bicarbonate (10 mL) and the aqueous phase was extracted with ethyl acetate (3 × 25 mL). The organic fractions were pooled together, washed with brine, and dried over $MgSO_4$. The volatiles were removed under reduced pressure and the crude solid was purified by flash column chromatography (silica; 40:60 (v/v) hexane/ethyl acetate), to yield 3-(2-fluoro-6-methoxyphenyl)-1*H*-pyrazole as a light yellow solid (2.21 g; 89%). ^{1}H NMR (400 MHz, $CDCl_3$) δ 11.56 (br, 1H; N*H*), 7.69 (d, *J* = 1.9 Hz, 1H; CHC*H*NH), 7.27 (td, *J* = 8.4, 6.8 Hz, 1H; *p*-Ar*H*), 6.91 – 6.82 (m, 3H; m-Ar*H* and C*H*CHNH), 4.02 (s, 3H; OCH_3). ^{13}C NMR (101 MHz, $CDCl_3$) δ 160.26 (d, *J* = 249.9 Hz; *C*-F), 157.17 (d, *J* = 6.9 Hz; *C*OMe), 139.54 (s; CH*C*HNH), 134.16 (s; *i*-Ar*C*), 128.95 (d, *J* = 11.5 Hz; *p*-Ar*C*), 109.29 (d, *J* = 23.8 Hz; *m*-Ar*C*), 107.11 (d, *J* = 3.0 Hz; *C*HCHNH), 106.91 (d, *J* = 12.9 Hz; *m*-Ar*C*), 56.43 (s; O*C*H_3). ^{19}F NMR (282 MHz, $CDCl_3$) δ -109.75.

3-(2-fluoro-6-hydroxyphenyl)-1*H*-pyrazole. 3-(2-fluoro-6-methoxyphenyl)-1*H*-pyrazole (1.6 g; 8.3 mmol) was dissolved in concentrated HBr (48%; 25 mL) and refluxed for ca. 24 h. The dark brown solution was cooled to 0° C and the pH adjusted to 7. The suspension was extracted with ethyl acetate (3 × 50 mL). The organic fractions were pooled together, washed with brine, and dried over $MgSO_4$. The volatiles were removed under reduced pressure and the crude solid was purified by flash column chromatography (silica; 40:60 (v/v) hexane/ethyl acetate). The resulting solid was subsequently sublimed under vacuum to yield 3-(2-fluoro-6-hydroxyphenyl)-1*H*-pyrazole as a white solid (1.1 g; 75%). ^{1}H NMR (400 MHz, CD_3CN) δ 11.60 (s, 2H; N*H* and O*H*), 7.82 (d, *J* = 2.5 Hz, 1H; CHC*H*NH), 7.21 (td, *J* = 8.3, 6.5 Hz, 1H; *p*-Ar*H*), 6.88 (dd, *J* = 5.1, 2.6 Hz, 1H; C*H*CHNH), 6.82 (dt, *J* = 8.3, 1.1 Hz, 1H; *m*-Ar*H*), 6.74 (ddd, *J* = 11.6, 8.2, 1.1 Hz, 1H; *m*-Ar*H*). ^{13}C NMR (101 MHz, CD_3CN) δ 160.88 (d, *J* = 246.9 Hz; *C*-F), 157.77 (d, *J* = 6.3 Hz; *C*OH), 146.16 (s; *i*-Ar*C*), 129.65 (d, *J* = 3.5 Hz; CH*C*HNH), 129.00 (d, *J* = 11.7 Hz; *p*-Ar*C*), 112.55 (d, *J* = 2.9 Hz; *m*-Ar*C*), 106.04 (d, *J* = 23.0 Hz; *m*-Ar*C*), 106.02 (s; *C*CHCHNH), 105.30 (d, *J* = 15.0 Hz; C*C*HCHNH). ^{19}F NMR (282 MHz, CD_3CN) δ -115.43 (dt, *J* = 11.6, 5.9 Hz). MS (m/z): calcd, 179.0621 $[M+H]^+$; found, 179.0592 (FAB+ , $[M+H]^+$).

2-(1H-pyrazol-3-yl)-3-fluorophenolate (NaOFArPzH). In the glovebox, to a solution of 3-(2-fluoro-6-hydroxyphenyl)-1*H*-pyrazole (1.1 g.; 6.2 mmol) in THF (10 mL) was added a solution of sodium bis(trimethylsilyl)amide (NaHMDS; 1.3 g; 7.0 mmol) in THF (2 mL). The homogenous solution was stirred for 2 h. where after solvent was removed under reduced pressure to yield a white solid. The solid was suspended in hexane (10 mL), collected on a medium porosity frit, washed with hexane (3 × 10.0 mL), and dried under reduced pressure to yield of sodium 2-(1*H*-pyrazol-3-yl)-3-fluorophenolate as an off-white powder. Yield 1.1 g (88%). ^{1}H NMR (400 MHz, CD_3CN) δ 13.98 (s, 1H, N*H*), 7.44 (d, *J* = 1.8 Hz, 1H, CHC*H*NH), 6.80 (q, *J* = 8.0 Hz, 1H, *p*-C*H*), 6.44 (dd, *J* = 5.5, 1.8 Hz, 1H, *m*-C*H*), 6.35 (dd, *J* = 8.4, 1.2 Hz, 1H, *m*-C*H*), 6.03 (ddd, *J* = 11.4, 8.0, 1.2 Hz, 1H, C*H*CHNH). ^{13}C NMR (101 MHz, CD_3CN) δ 171.10 (d, *J* = 6.7 Hz, *C*-OH), 161.63 (d, *J* = 244.0 Hz, *C*-F), 141.09 (s, *i*-Ar*C*), 137.90 (s, CH*C*HNH), 127.01 (d, *J* = 13.8 Hz, *p*-ArC), 117.19 (d, *J* = 2.0 Hz; m-Ar*C*), 106.47 (*C*CHCHNH), 102.23 (d, *J* = 12.3 Hz, (*m*-Ar*C*), 96.64 (d, *J* = 23.3 Hz, *C*HCHNH). ^{19}F NMR (282 MHz, CD_3CN) δ -115.73 (m).

3-(2,6-difluorophenyl)-1*H*-pyrazole. Under N_2, a Schlenk-tube was charged with 2,6-difluoroacetophenone (2.60 mL; 20.0 mmol) and *N,N*-dimethylformamide dimethylacetal (2.65 mL; 20.0 mmol). The tube was sealed and heated at 110° C for ca. 16 h. Next, the volatiles were removed under reduced pressure to yield an orange oil (1-(2,6-difluorophenyl)-3-(dimethylamino)-prop-2-en-1-one). The crude oil was used without further purification and dissolved in ethanol (15 mL). To the solution was added hydrazine monohydrate (1.1 mL; 22.7 mmol) and acetic acid (1.3 mL; 22.8 mmol). The mixture was stirred for 3 h. at 50° C, during which the color changed from orange to yellow. Hereafter, the ethanol was removed under reduced pressure and the remaining oil was dissolved in ethyl acetate (10 mL). To the solution was added sat. sodium bicarbonate (25 mL) and the aqueous phase was extracted with ethyl acetate (3 × 25 mL). The organic fractions were pooled together, washed with brine, and dried over $MgSO_4$. The volatiles were removed under reduced pressure and the crude solid was purified by flash column chromatography (silica; 40:60 (v/v) hexane/ethyl acetate). The resulting solid was subsequently sublimed under vacuum to yield 3-(2,6-difluorophenyl)-1*H*-pyrazole as a light yellow solid (2.70 g; 75%). ^{1}H NMR (400 MHz, CD_3CN) δ 11.49 (s, 1H; N*H*), 7.73 (d, *J* = 2.2 Hz, 1H; CHC*H*NH), 7.41 (tt, *J* = 8.2, 6.3 Hz, 1H; *p*-Ar*H*), 7.17 – 7.03 (m, 2H; *m*-Ar*H*), 6.67 (m, *J* = 2.0 Hz, 1H; C*H*CHNH). ^{13}C NMR (101 MHz, CD_3CN) δ 160.09 (dd, *J* = 249.1, 7.3 Hz; *C*-F), 132.75 (s; *i*-Ar*C*) 129.75 (t, *J* = 10.7 Hz; *p*-Ar*C*), 113.92 – 109.90 (m; *m*-Ar*C*), 110.11 (s; *C*CHCHNH), 106.84 (t, *J* = 4.0 Hz; C*C*HCHN). ^{19}F NMR (282 MHz, CD_3CN) δ -113.39. MS (m/z): calcd, 181.0577 $[M+H]^+$; found, 181.0587 (FAB+ , $[M+H]^+$).

Sodium 3-(2,6-difluorophenyl)pyrazolate (NaF_2ArPz). In the glovebox, to a solution of 3-(2,6-difluorophenyl)-1*H*-pyrazole (2.70 g.; 15.0 mmol) in THF (20 mL) was added a solution of sodium bis(trimethylsilyl)amide (3.00 g; 18.0 mmol) in THF (5 mL). The color darkens to light yellow and the homogenous solution was stirred for 2 h. The solvent was removed under reduced pressure to yield a yellow foam. Addition of hexane (10.0 mL) resulted in the formation of a white precipitate, which was collected on a medium porosity frit. The solid was washed with hexane (3 × 20.0 mL) and dried under reduced pressure to yield of sodium 3-(2,6-difluorophenyl)-pyrazolate (2.90 g; 95%) as an off-white powder. ^{1}H NMR (400 MHz, CD_3CN) δ 7.53 (d, *J* = 1.6 Hz, 1H, CHC*H*N), 7.21 – 7.09 (m, 1H, *p*-Ar*H*), 7.03 – 6.90 (m, 2H, m-Ar*H*), 6.42 (td, *J* = 2.6, 1.6 Hz, 1H, C*H*CHN). ^{13}C NMR (101 MHz, CD_3CN) δ 159.94 (dd, *J* = 244.7, 8.9 Hz, *C*-F), 138,92 (s, *C*CHCHN), 138.88 (t, *J* = 2.8, 1.9 Hz, CH*C*HN), 125.90 (t, *J* = 11.0 Hz, *p*-Ar*C*), 115.08 (t, *J* = 17.3 Hz, *i*-Ar*C*), 113.68 – 109.65 (m, *m*-Ar*C*), 104.44 (t, *J* = 4.1 Hz, *C*HCHN). ^{19}F NMR (282 MHz, CD_3CN) δ -114.69 – -114.85 (m).

2-(1H-pyrazol-3-yl)phenolate (NaOArPzH). In the glovebox, to a solution of 3-(2-hydroxyphenyl)-1*H*-pyrazole (480 mg.; 3.0 mmol) in THF (10 mL) was added a solution of sodium bis(trimethylsilyl)amide (550 mg; 3.0 mmol) in THF (2 mL). The homogenous solution was stirred for 2 h. where after solvent was removed under reduced pressure to yield a white solid. The solid was suspended in hexane (10 mL), collected on a medium porosity frit, washed with hexane (3 × 10.0 mL), and dried under reduced pressure to yield of sodium 2-(1*H*-pyrazol-3-yl)phenolate (475 mg; 87%) as an off-white powder. ^{1}H NMR (400 MHz, CD_3CN) δ 7.42 (dd, *J* = 7.3, 1.9 Hz, 2H; *o*-Ar*H* and CHC*H*NH), 6.93 (ddd, *J* = 8.4, 6.9, 1.9 Hz, 1H; *p*-Ar*H*), 6.61 (dt, *J* = 8.3, 1.0 Hz, 1H; *m*-Ar*H*), 6.42 (dd, *J* = 2.0, 0.7 Hz, 1H; C*H*CHNH), 6.36 – 6.27 (m, 1H; *m*-Ar*H*). ^{13}C NMR (101 MHz, CD_3CN) δ 168.75 (*C*-OH), 146.74 (*i*-Ar*C*), 137.40 (CCH*C*HNH), 128.32 (*p*-Ar*C*), 126.24 (*o*-Ar*C*), 121.59 (*m*-Ar*C*), 117.12 (*C*CHCHNH), 110.56 (*m*-Ar*C*), 97.62 (C*C*HCHNH).

$[LFe_3(PhPz)_2(OArPz)OFe][OTf]_1$ (3); Method A. In the glovebox, to a solution of $[LFe_3(PhPz)_3OFe][OTf]_2$ (184.6 mg; 0.10 mmol) in CH_2Cl_2 (8.0 mL) was added a suspension 2-(1*H*-pyrazol-3-yl)-3-phenolate (NaOArPzH; 20.5 mg; 0.11 mmol) in CH_2Cl_2 (1.0 mL). The solution was stirred for ca. 48 h., during which the color changed from brown to red/brown. The solution was filtered over a bed of Celite (0.5 cm) in a glass pipette and the solvent removed under reduced pressure. The red/brown solid (173 mg) was crystallized from CH_2Cl_2/Et_2O to yield $[LFe_3(PhPz)_2(OPhPz)OFe][OTf]_1$ as a red/brown solid. Yield 129 mg (78%). ^{1}H NMR (300

MHz, CD_2Cl_2) δ 122.0 (br), 120.4 (br), 117.6 (br), 86.4 (br), 79.6 (br), 74.5 (s), 72.8 (s), 72.0 (s), 67.1 (s), 61.5 (s), 55.5 (s), 54.2 (s), 51.0 (br), 48.5 (s), 46.9 (s), 45.3 (s), 42.7 (s), 37.8 (s), 35.8 (s), 30.3 (s), 27.3 (s), 26.6 (s), 26.2 (s), 25.3 (s), -2.9 (br), -4.9 (s), -11.0 (br), -15.0 (s), -39.9 (br). ^{19}F NMR (282 MHz, CD_2Cl_2) δ -78.8. UV-Vis (CH_2Cl_2) [ε (M^{-1} cm^{-1})]: 253 nm (8.41×10^4), 309 nm (1.84×10^3), 498 (6.15×10^3). Anal. calcd. (%) for $C_{85}H_{59}F_3Fe_4N_{12}O_8S_1$: C 60.45, H 3.52, N 9.95; found: C 59.76, H 3.54, N 9.53.

$[LFe_3(PhPz)_2(OArPz)OFe][OTf]_1$ (3); Method B. In the glovebox, to a solution of $[LFe_3(PhPz)_2(OArPz)OFe][OTf]_2$ (36.9 mg, 0.02 mmol; from method A) in CH_2Cl_2 (3 mL), was added a solution of cobaltocene ($CoCp_2$, 3.8 mg, 0.02 mmol) in CH_2Cl_2 (1 mL). Upon addition the reaction mixture changed color from green/black to red/brown immediately. The reaction mixture was stirred for 2 h, and the volatiles were removed under reduced pressure. NMR analysis of the crude reaction mixture revealed > 90% conversion to $[LFe_3(PhPz)_2(OPhPz)OFe][OTf]_1$. A small paramagnetic impurity is present and is of unknown identity. ^1H NMR is identical to that of $[LFe_3(PhPz)_2(OArPz)OFe][OTf]_1$ (Figure S18).

$[LFe_3(PhPz)_2(OArPz)OFe][OTf]_2$ (2); Method A. In the glovebox, to a solution of $[LFe_3(PhPz)_3OFe][OTf]_2$ (367.0 mg; 0.2 mmol) in CH_2Cl_2 (15 mL), was added a suspension of iodosobenzene (PhIO; 50.0 mg; 0.23 mmol) as a solid. The resulting suspension was stirred for ca. 16 h. where upon the mixture became a homogenous green/black solution. The volatiles were removed under reduced pressure to yield a crude black solid (342.2 mg), which was mainly $[LFe_3(PhPz)_2(OArPz)OFe][OTf]_2$ as judged by ^1H NMR. The crude solid was crystallized from MeCN/Et_2O to give $[LFe_3(PhPz)_2(OArPz)OFe][OTf]_2$ as black crystals. Yield 190 mg (52%). ^1H NMR (300 MHz, CD_2Cl_2) δ 146.2 (br), 140.0 (br), 119.9 (br), 111.5 (br), 105.5 (br), 88.6 (s), 81.8 (s), 80.6 (s), 75.6 (s), 72.4 (s), 68.6 (s), 65.0 (s), 64.6 (s), 63.9 (s), 54.6 (s), 49.7 (s), 47.7 (s), 38.8 (s), 30.4 (s), 30.0 (s), 26.6 (s), 18.4 (s), 16.3 (s), 14.7 (s), 12.0 (s), 10.8 (s), -4.8 (br), -6.7 (br), -9.9 (s), -19.3 (s), -25.5 (br). ^{19}F NMR (282 MHz, CD_2Cl_2) δ -78.1. UV-Vis (CH_2Cl_2) [ε (M^{-1} cm^{-1})]: 244 nm (9.37×10^4), 366 nm (8.99×10^3), 462 nm (6.53×10^3). Anal. calcd. (%) for $C_{86}H_{59}F_6Fe_4N_{12}O_{11}S_2$: C 56.20, H 3.24, N 9.15; found: C 55.83, H 3.12, N 8.78.

$[LFe_3(PhPz)_2(OArPz)OFe][OTf]_2$ (2); Method B. In the glovebox, to a solution of $[LFe_3(PhPz)_3OFe][OTf]_3$ (200.6 mg; 0.10 mmol) in CH_2Cl_2 (8.0 mL) was added a suspension 2-(1*H*-pyrazol-3-yl)-3-phenolate (NaOArPzH; 20.4 mg; 0.11 mmol) in CH_2Cl_2 (1.0 mL). The solution was stirred for ca. 48 h., during which the color changed from brown to green/black. The

solution was filtered over a bed of Celite (0.5 cm) in a glass pipette and the solvent removed under reduced pressure. The black solid (181 mg) was crystallized from MeCN/Et_2O to give $[LFe_3(PhPz)_2(OArPz)OFe][OTf]_2$ as a black crystals. Yield 91 mg (49%). The ^1H NMR was identical to that of Method A (Figure S21). Note that a small impurity ($[LFe_3(PhPz)_3OFe][OTf]_2$) remained present, even upon repeated recrystallization.

$[LFe_3(PhPz)_2(OArPz)OFe][OTf]_2$ (2); Method C. In the glovebox, to a rapidly stirred solution of $[LFe_3(PhPz)_2(OArPz)OFe][OTf]_1$ (23 mg, 0.013 mmol) in CH_2Cl_2 (2.0 mL) was added silver triflate (AgOTf; 3.9 mg, 0.015 mmol) as a suspension in CH_2Cl_2 (1.0 mL). The solution was stirred for 2 h., during which the color changed from red/brown to green/black. The solution was filtered over a bed of Celite (0.5 cm) in a glass pipette, and solvent was removed under reduced pressure to yield $[LFe_3(PhPz)_2(OArPz)OFe][OTf]_2$ as a black solid. Yield 19 mg (79%). The ^1H NMR was identical to that of Method A (Figure S21). Note, the paramagnetic peaks between 25-30 ppm are fluxional, and deviate slightly from method A.

$[LFe_3(PhPz)_2(OArPz)OFe][OTf]_2$ (2); Method D. In the glovebox, to a stirring solution of $[LFe_3(PhPz)_3OFe][OTf]_2$ (90.9 mg, 0.05 mmol) in DCM (2.0 mL) was added a solution of tetrabutylammoniun periodate ($^nBu_4NIO_4$; 22.1 mg, 0.05 mmol) in DCM (1.0 mL). The yellow brown solution turned green/black immediately and after 30 minutes the solvents were removed under reduced pressure to yield a crude black solid (95.2 mg). The ^1H NMR was identical to that of Method C (Figure S22).

$[LFe_3(F_2ArPz)_3OFe][OTf]_1$ (4). In the glovebox, a suspension of $LFe_3(OAc)(OTf)_2$ (4143 mg, 3.0 mmol) in THF (125 mL) is frozen in the cold well. To the thawing suspension is added sodium 2,6-difluorophenylpyrazolate (NaF_2ArPz; 2011 mg, 10.0 mmol) in THF (10 mL). The color changed immediately to orange and the suspension became homogeneous during the course of 1 hour. The solution was stirred for a total of 2 h, and a yellow/brown suspension was formed. Next, iodosobenzene (PhIO, 660 mg, 3.0 mmol) was added as a solid, and the suspension turned dark brown and homogeneous. After 1 h, iron(II) trifluoromethane sulfonate ($Fe(OTf)_2$; 2192, 6.0 mmol) was added, and the solution was stirred for ca. 16 h. Hereafter, the volatiles were removed under reduced pressure, and the remaining brown solid was redissolved in CH_2Cl_2 (125 mL). To the solution was added cobaltocene ($CoCp_2$; 1200 mg; 6.0 mmol) and stirred for another 2 h, during which the color changed to red/brown. The volatiles were removed under reduced pressure and the remaining solid was washed with ether (20 mL), toluene (20 mL), and thoroughly with

dimethoxyethane (DME; 150 mL) on a medium porosity glass frit. The remaining red solid was collected and dried under vacuum to yield $[LFe_3(F_2ArPz)_3OFe][OTf]_1$ as a red solid. Yield 1960 mg (37%). ^{1}H NMR (300 MHz, CD_2Cl_2) δ 97.2 (br), 60.2 (s), 56.5 (s), 36.4 (s), 34.3 (s), 33.8 (s), 29.3 (br), 24.3 (s), 15.5 (s), 13.4 (s), 13.1 (s), 9.5 (s), -3.6 (br), -8.0 (br). ^{19}F NMR (282 MHz, CD_2Cl_2) δ -78.8. UV-Vis (CH_2Cl_2) [ε (M^{-1} cm^{-1})]: 252 nm (9.14×10^4), 350 nm (5.03×10^3), 507 nm (3.3×10^3). Anal. calcd. (%) for $C_{85}H_{54}F_9Fe_4N_{12}O_7S_1$: C 57.30, H 3.05, N 9.43; found: C 57.44, H 2.99, N 9.36.

$[LFe_3(F_2ArPz)_3OFe][OTf]_2$ (5). In the glovebox, to a rapidly stirred solution of $[LFe_3(F_2ArPz)_3OFe][OTf]_1$ (1960 mg, 1.1 mmol) in CH_2Cl_2 (50 mL) was added silver triflate (AgOTf; 312 mg, 1.1 mmol) as a solid. The solution was stirred for 2 h., during which the color changed from red/purple to brown. The solution was filtered over a bed of Celite (0.5 cm) on a medium porosity glass frit, and solvent was removed under reduced pressure to yield $[LFe_3(F_2ArPz)_3OFe][OTf]_2$ as a brown solid. Yield 1496 mg (70%). ^{1}H NMR (300 MHz, CD_2Cl_2) δ 116.6 (br), 70.5 (s), 67.6 (s), 55.9 (br), 49.0 (s), 44.3 (s), 43.7 (s), 15.6 (s), 14.4 (s), 14.2 (s), 12.8 (s), 1.7 (br), -3.2 (br). ^{19}F NMR (282 MHz, CD_2Cl_2) δ -77.5. UV-Vis (CH_2Cl_2) [ε (M^{-1} cm^{-1})]: 244 nm (9.28×10^4), 419 nm (6.18×10^3). Anal. calcd. (%) for $C_{86}H_{54}F_{12}Fe_4N_{12}O_{10}S_2$: C 53.49, H 2.82, N 8.70; found: C 52.71, H 2.66, N 8.66.

Reaction of Iodosylbenzene (PhIO) and $[LFe_3(F_2ArPz)_3OFe][OTf]_2$. In the glovebox, to a solution of $[LFe_3(F_2ArPz)_3OFe(F)][OTf]_2$ (20.0 mg; 0.01 mmol) in CH_2Cl_2 (2.0 mL) was added a suspension of iodosobenzene (PhIO; 2.2 mg; 0.01 mmol) in CH_2Cl_2 (1.0 mL). The mixture was stirred for ca. 16 h., and the solvent was removed under reduced pressure. ^{1}H NMR of the crude reaction product showed the formation of two distinct species, identified by ESI-MS as: (i) $[LFe_3(F_2ArPz)_2(FPhPz)OFe(O)]^{2+}$ (**7**; *m/z* = 814.1) and (ii) $[LFe_3(F_2ArPz)_3OFe(F)]^{2+}$ (**8**; m/z = 825.6); see Figure S37. Based on the relative integration of the peaks at 118.3 (**7**) and 107.3 ppm (**8**) in the crude reaction mixture – vs. a known 1:1 ratio of **7** and **8** – the relative ratios of **7** and **8** are approximately 45:55 (**7**:**8**). Together with **7** and **8** a paramagnetic impurity is present and is of unknown identity. The species **7** and **8** were independently synthesized for identification, structural characterization, and confirmation of C–F bond activation with concomitant transfer of a fluorine anion (*vide infra*).

$[LFe_3(F_2ArPz)_2(OFArPz)OFe][OTf]_1$ (6). In the glovebox, to a solution of $[LFe_3(F_2ArPz)_3OFe][OTf]_2$ (97.5 mg; 0.052 mmol) in CH_2Cl_2 (4.0 mL) was added a suspension

2-(1*H*-pyrazol-3-yl)-3-fluorophenolate (NaOFArPzH; 12.3 mg; 0.61 mmol) in CH_2Cl_2 (1.0 mL). The solution was stirred for ca. 24 h., during which the color changed from brown to red/brown. The solution was filtered over a bed of Celite (0.5 cm) in a glass pipette and the solvent removed under reduced pressure. The red/brown solid (94 mg) was crystallized from MeCN/Et_2O to yield $[LFe_3(F_2ArPz)_2(OFArPz)OFe][OTf]_1$ as red/brown crystals. Yield 47 mg (51%). ^{1}H NMR (300 MHz, CD_2Cl_2) δ 128.6 (br), 126.0 (br), 122.7 (br), 91.2 (br), 86.0 (br), 75.7 (s), 75.2 (s), 74.3 (s), 73.2 (s), 69.8 (s), 68.2 (s), 66.0 (br), 58.0 (s), 56.4 (s), 50.9 (s), 50.2 (s), 48.8 (s), 45.1 (s), 36.16 (s), 35.7 (s), 34.6 (s), 30.7 (s), 30.0 (s), 24.5 (s), 24.1 (s), 18.5 (s), 14.7 (s), 13.3 (s), 13.3 (s), 12.6 (s), 12.4 (s), 10.1 (s), 9.5 (s), 9.0 (s), -7.4 (br), -11.3 (br), -19.0 (s), -33.7 (br). ^{19}F NMR (282 MHz, CD_2Cl_2) δ -47.5, -58.5, -75.1, -78.7, -82.3, -98.8. UV-Vis (CH_2Cl_2) [ε (M^{-1} cm^{-1})]: 245 nm (12.21×10^4), 302 nm (2.41×10^4), 500 nm (7.32×10^3). Anal. calcd. (%) for $C_{85}H_{54}F_8Fe_4N_{12}O_8S_1$: C 57.39, H 3.06, N 9.45; found: After several attempts, no suitable EA has been obtained yet.

$[LFe_3(F_2ArPz)_2(OFArPz)OFe][OTf]_2$ (7) Method A. In the glovebox, to a rapidly stirred solution of $[LFe_3(F_2ArPz)_2(OFArPz)OFe][OTf]_1$ (90 mg, 0.05 mmol) in CH_2Cl_2 (5.0 mL) was added silver triflate (AgOTf; 12.4 mg, 0.05 mmol) as a suspension in CH_2Cl_2 (1.0 mL). The solution was stirred for 2 h., during which the color changed from red/brown to green/black. The solution was filtered over a bed of Celite (0.5 cm) in a glass pipette, and the solvent was removed under reduced pressure to yield a crude black solid (89 mg). The black solid (70 mg) was recrystallized from MeCN/Et_2O to $[LFe_3(F_2ArPz)_2(OFArPz)OFe][OTf]_2$ as black crystals. Yield 37.4 mg (53%). ^{1}H NMR (300 MHz, CD_2Cl_2) δ 154.1 (br), 145.3 (br), 131.1 (br), 117.4 (br), 106.7 (br), 91.6 (br), 84.6 (s), 82.8 (s), 82.3 (s), 77.5 (s), 71.2 (s), 70.6 (s), 68.2 (s), 67.0 (s), 64.9 (s), 61.5 (s), 56.6 (s), 47.9 (s), 40.4 (s), 38.1 (s), 35.5 (s), 30.5 (s), 16.7 (s), 15.5 (s), 15.4 (s), 15.2 (s), 14.1 (s), 12.8 (s), 12.4 (s), 11.4 (s), 10.3 (s), 9.9 (s), -1.4 (br), -4.4 (br), -9.1 (br) , -17.4 (br), -22.6 (s). ^{19}F NMR (282 MHz, CD_2Cl_2) δ -46.9, -66.5, -67.3, -78.0, -79.3, -103.6, -110.8, -111.5. UV-Vis (CH_2Cl_2) [ε (M^{-1} cm^{-1})]: 242 nm (10.73×10^4), 345 nm (1.22×10^4), 430 nm (8.35×10^3), 582 nm (4.58×10^3). Anal. calcd. (%) for $C_{86}H_{54}F_{11}Fe_4N_{12}O_{11}S_2$: C 53.58, H 2.82, N 8.72; found: C 53.29, H 3.11, N 8.56.

$[LFe_3(F_2ArPz)_2(OFArPz)OFe][OTf]_2$ (7) Method B. In the glovebox, to a stirring solution of $[LFe_3(F_2ArPz)_3OFe][OTf]_2$ (203.1 mg, 0.1 mmol) in DCM (8.0 mL) was added a solution of tetrabutylammoniun periodate ($^nBu_4NIO_4$; 46.2 mg, 0.1 mmol) in DCM (1.0 mL). The yellow brown solution turned green/black immediately and after 30 minutes the solvents were removed

under reduced pressure to yield a crude black solid (217 mg). The ^{1}H NMR of the crude solid is similar to that of $[LFe_3(F_2ArPz)_2(OFArPz)OFe][OTf]_2$, although a small paramagnetic impurity is present (Figure S30). No $[LFe_3(F_2ArPz)_3OFe(F)][OTf]_2$ (**8**) was detected by ^{1}H NMR, most likely due to the near immediate conversion of **5** to **7**.

$[LFe_3(F_2ArPz)_3OFe(F)][OTf]_2$ (8). In the glovebox, to a solution of $[LFe_3(F_2ArPz)_3OFe][OTf]_2$ (380.0 mg; 0.2 mmol) in acetonitrile (10 mL) was added a solution of xenon difluoride (XeF_2; 40.0 mg.; 0.23 mmol) in acetonitrile (2 mL). The solution darkened immediately to dark brown and was stirred for an additional 2h. The volatiles were removed under reduced pressure to give give **[**$LFe_3(F_2ArPz)_3OFe(F)][OTf]_2$ as crude brown solid (374 mg > 95% conversion by ^{1}H NMR). Crystallization from DCM/Et_2O only gave a few poor crystals suitable for X-ray analyses. Crystallization of the crude brown solid (4 x 30 mg) from CH_2Cl_2/C_6H_6 gave brown crystals. Yield 68.9 mg (57%). ^{1}H NMR (300 MHz, CD_2Cl_2) δ 145.8 (br), 107.4 (br), 85.6 (s), 67.3 (s), 64.4 (s), 44.7 (s), 16.0 (s), 12.8 (s), 11.6 (s), 11.0 (s), 10.1 (s), -1.6 (s), -10.7 (s). ^{19}F NMR (282 MHz, CD_2Cl_2) δ -72.0, -77.0, -80.6. UV-Vis (CH_2Cl_2) [ε (M^{-1} cm^{-1})]: 243 nm (9.57×10^4), 357 nm (9.34×10^3), 437 nm (6.88×10^3). Anal. calcd. (%) for $C_{86}H_{54}F_{13}Fe_4N_{12}O_{10}S_2$: C 52.97, H 2.79, N 8.62; found: After several attempts, no suitable EA has been obtained yet.

Reaction of PhIO with Sodium 3-phenylpyrazolate. In the glovebox, to a suspension of iodosobenzene (PhIO; 22.5 mg; 0.1 mmol) in 2 mL THF was added a solution of sodium 3-phenylpyrazolate (NaPhPz; 16.7 mg; 0.1 mmol) in 3 mL THF. The resulting suspension was stirred for 16 h, and remained a suspension throughout. The mixture was divided into two portions (2 × 2.5 mL). The first 2.5 mL fraction was filtered and the solvent was removed under reduced pressure to yield 10.2 mg of a crude solid. ^{1}H NMR (in CD_3CN + 5 μL CH_2Cl_2 as internal standard) of the crude solid did not indicate hydroxylation of the pyrazole ligand (Figure S30). Based on the internal standard the yield, was 5.0 mg (60%). From the second 2.5 mL fraction, the solvent was removed under reduced pressure to yield 21.0 mg of crude solid. Outside the glovebox, to the solid was added 1.0 mL MeOH, 1.0 mL THF, 1.0 mL H2O, 0.5 mL NH_4Cl (sat.), and subsequently solubilized. The solution was filtered over alumina and analyzed by gas chromatography mass spectroscopy (GC-MS). GC-MS did not show any peak of the pyrazole ligand.

Reaction of PhIO with Sodium 3-(2,6-difluorophenyl)pyrazolate. In the glovebox, to a suspension of iodosobenzene (PhIO; 22.2 mg; 0.1 mmol) in 2 mL THF was added a solution of

sodium 3-(2,6-difluorophenyl)pyrazolate (NaF_2ArPz; 20.2 mg; 0.1 mmol) in 3 mL THF. The resulting suspension was stirred for 16 h, and remained a suspension throughout. The mixture was divided into two portions (2 × 2.5 mL). The first 2.5 mL fraction was filtered and the solvent was removed under reduced pressure to yield 9.9 mg of a crude solid. ^{1}H NMR (in CD_3CN + 5 μL CH_2Cl_2 as internal standard) of the crude solid did not indicate hydroxylation of the pyrazole ligand (Figure S31). Based on the internal standard the yield, was 9.0 mg (90%). After NMR analysis, outside the glovebox, to the NMR sample was added 1.0 mL H_2O, 0.2 mL HCl (conc.), 0.2 mL NaOH (9M). The solution was extracted with CH_2Cl_2 (2 × 1.0 mL), and the organic fraction was filtered over alumina and analyzed by gas chromatography mass spectroscopy (GC-MS). GC-MS did not show any peak of the pyrazole ligand.

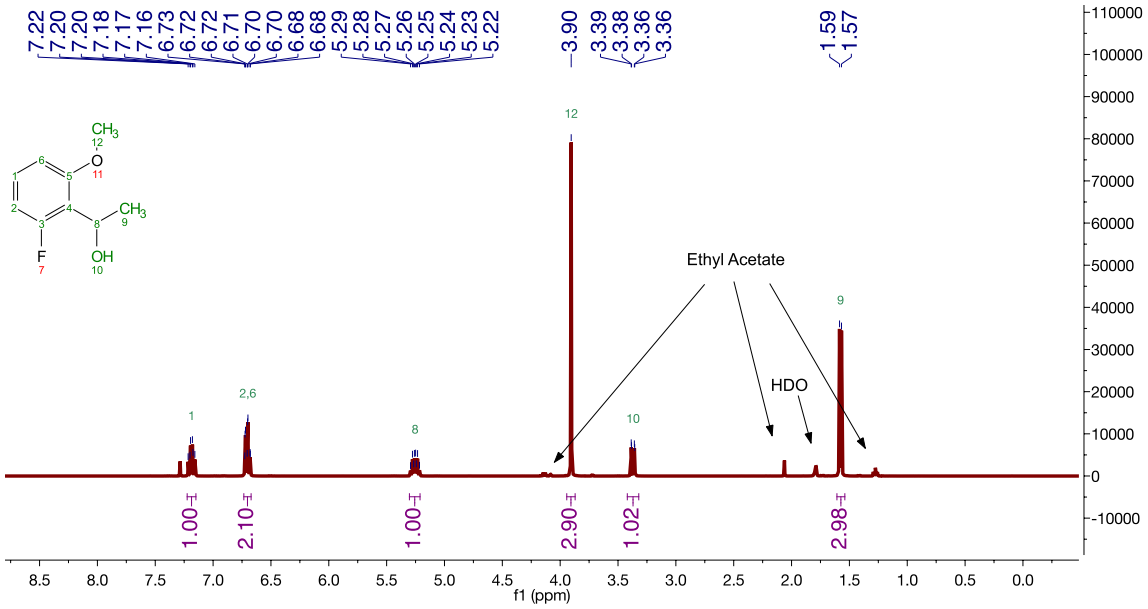

Figure S1. ^{1}H NMR spectrum (400 MHz) of 1-(2-fluoro-6-methoxyphenyl)ethan-1-ol in $CDCl_3$.

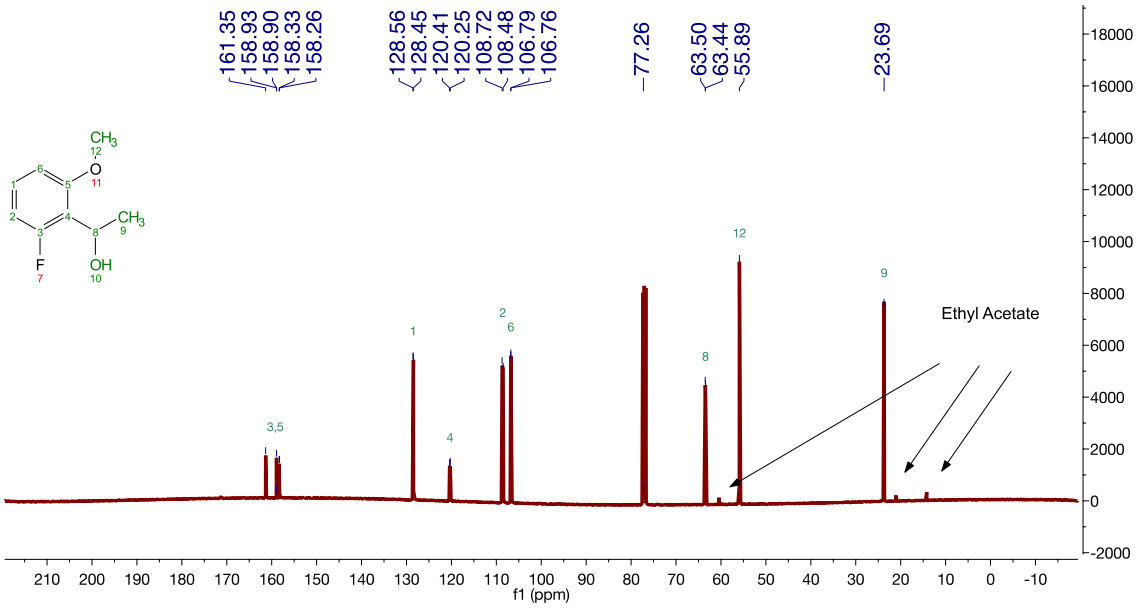

Figure S2. ^{13}C NMR spectrum (400 MHz) of 1-(2-fluoro-6-methoxyphenyl)ethan-1-ol in $CDCl_3$.

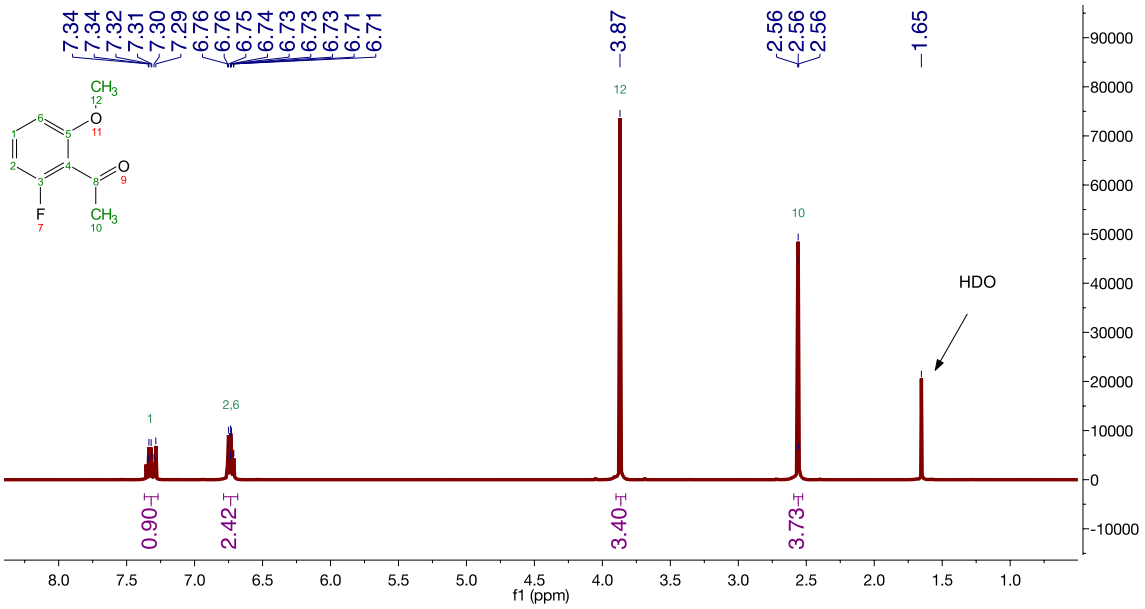

Figure S3. ^{1}H NMR spectrum (400 MHz) of 2-fluoro-6-methoxyacetophenone in $CDCl_3$.

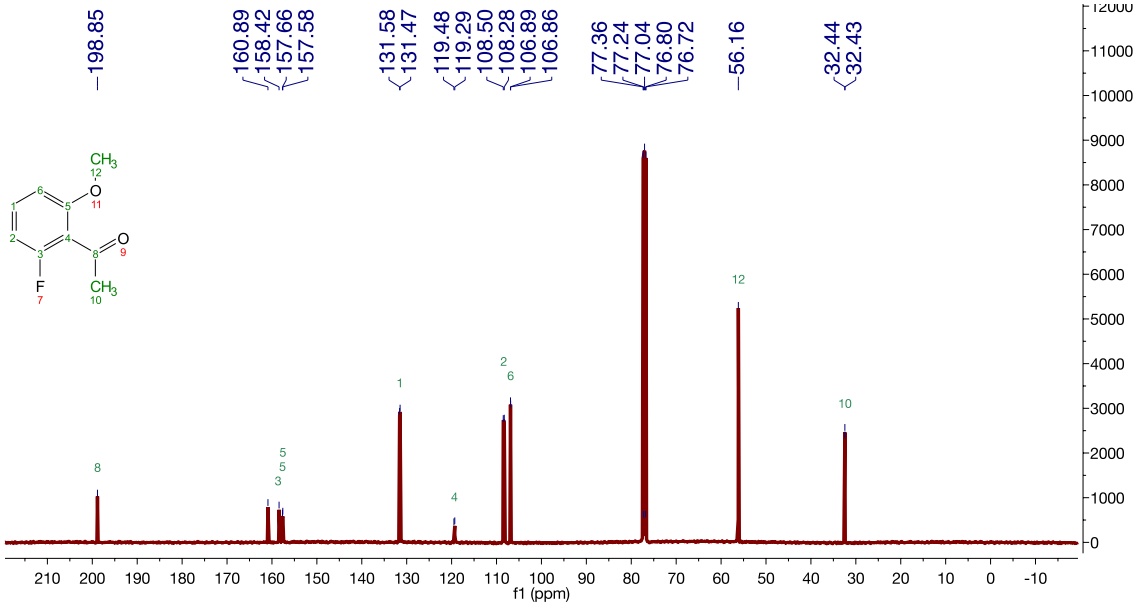

Figure S4. ^{13}C NMR spectrum (400 MHz) of 2-fluoro-6-methoxyacetophenone in $CDCl_3$.

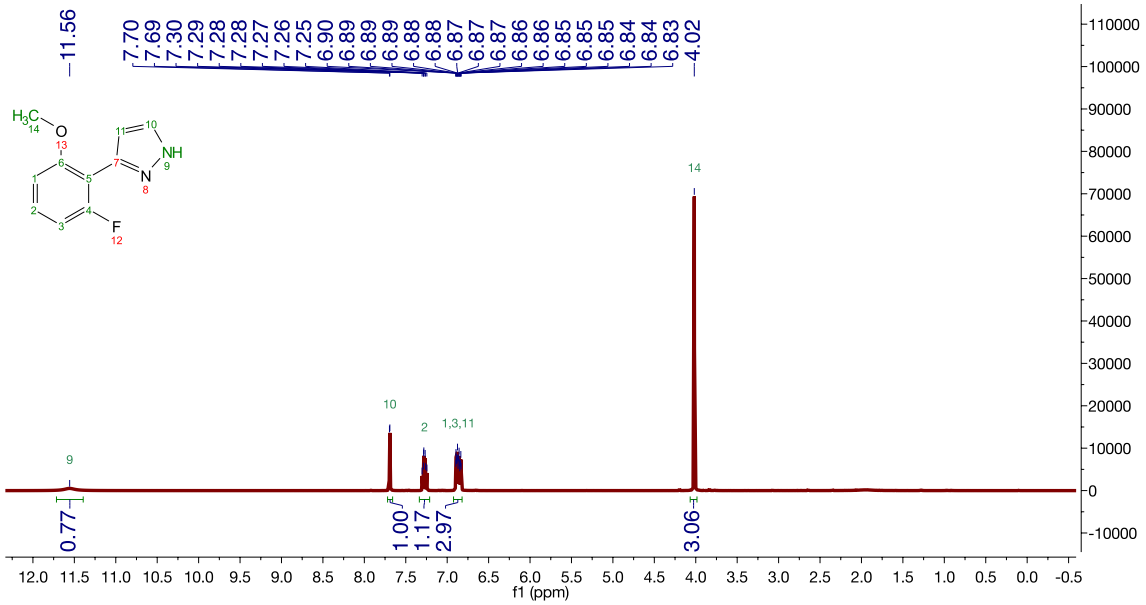

Figure S5. ^{1}H NMR spectrum (400 MHz) of 3-(2-fluoro-6-methoxyphenyl)-1*H*-pyrazole in $CDCl_3$.

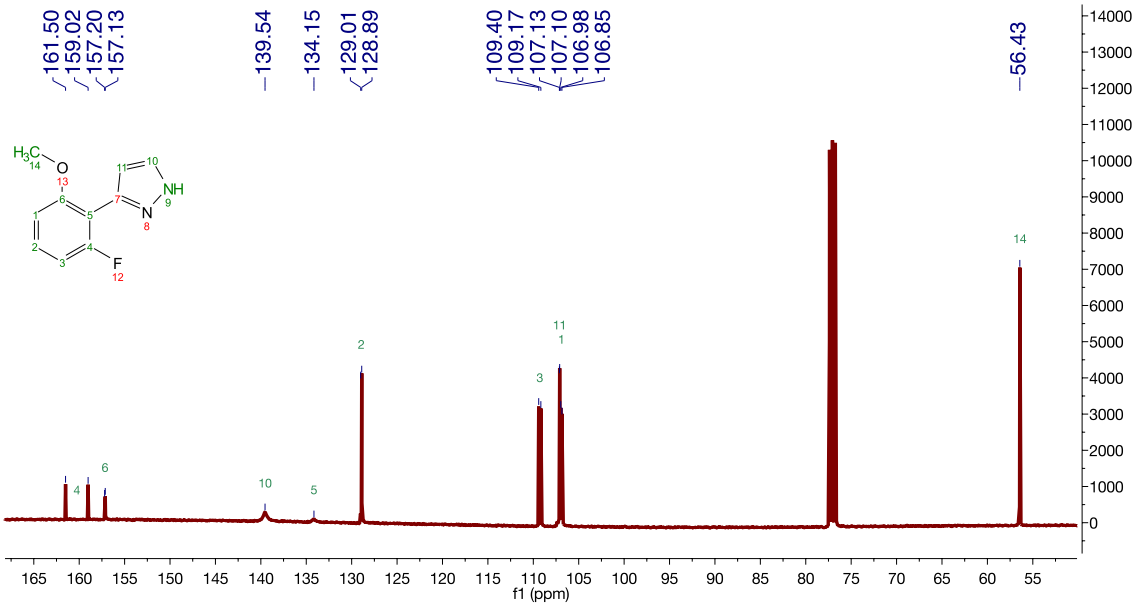

Figure S6. ^{13}C NMR spectrum (400 MHz) of 3-(2-fluoro-6-methoxyphenyl)-1*H*-pyrazole in $CDCl_3$.

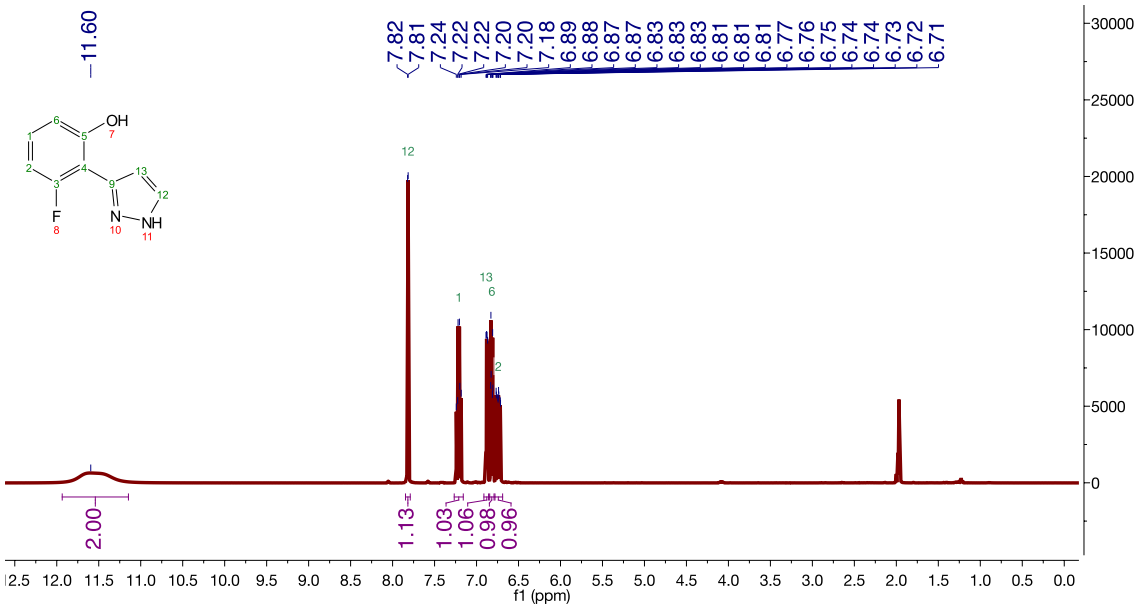

Figure S7. ^{1}H NMR spectrum (400 MHz) of 3-(2-fluoro-6-hydroxyphenyl)-1*H*-pyrazole in CD_3CN.

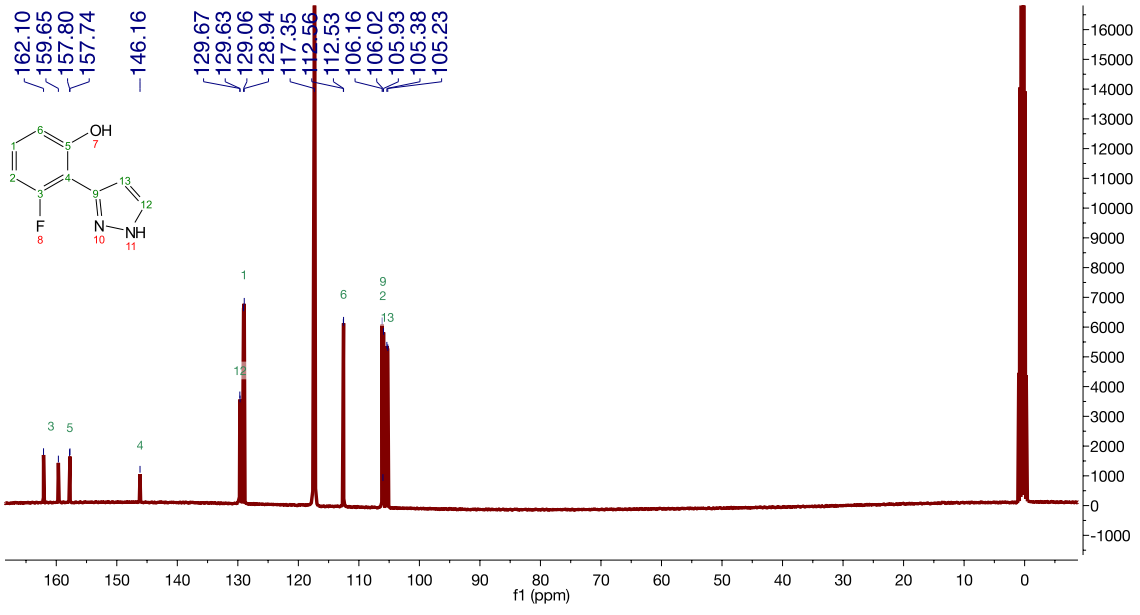

Figure S8. ^{13}C NMR spectrum (400 MHz) of 3-(2-fluoro-6-hydroxyphenyl)-1*H*-pyrazole in CD_3CN.

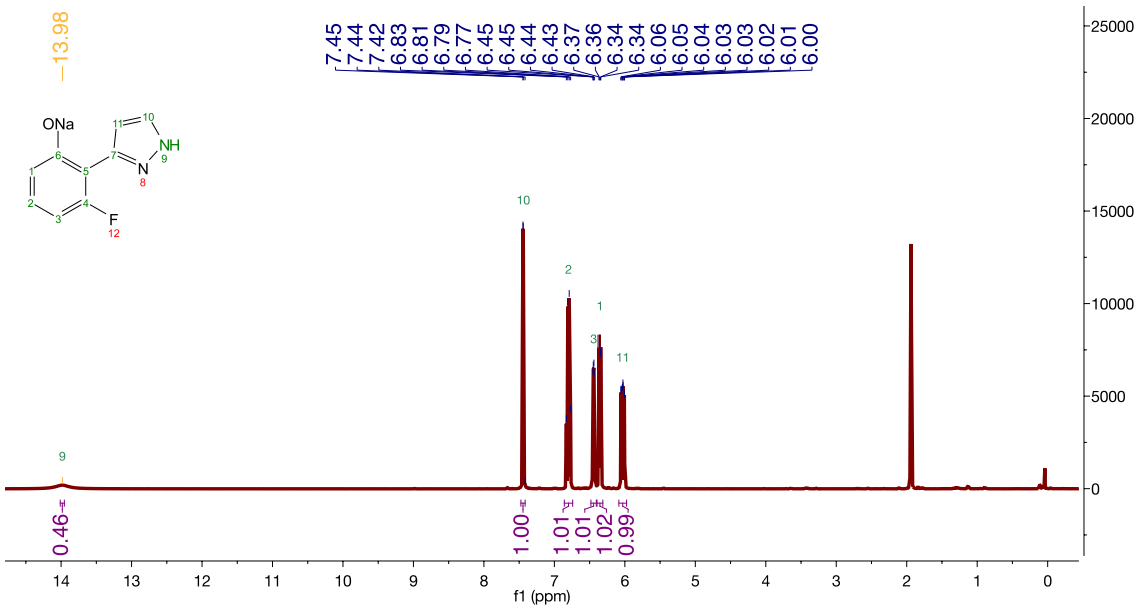

Figure S9. ^{1}H NMR spectrum (400 MHz) of sodium 2-(1H-pyrazol-3-yl)-3-fluorophenolate in CD_3CN.

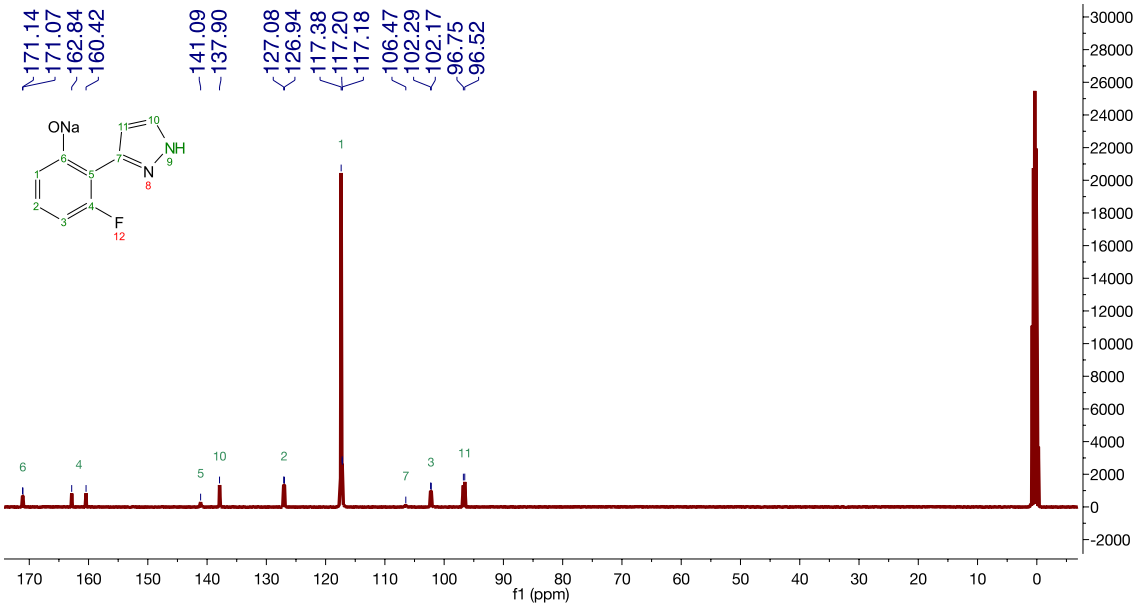

Figure S10. ^{13}C NMR spectrum (400 MHz) of sodium 2-(1H-pyrazol-3-yl)-3-fluorophenolate in CD_3CN.

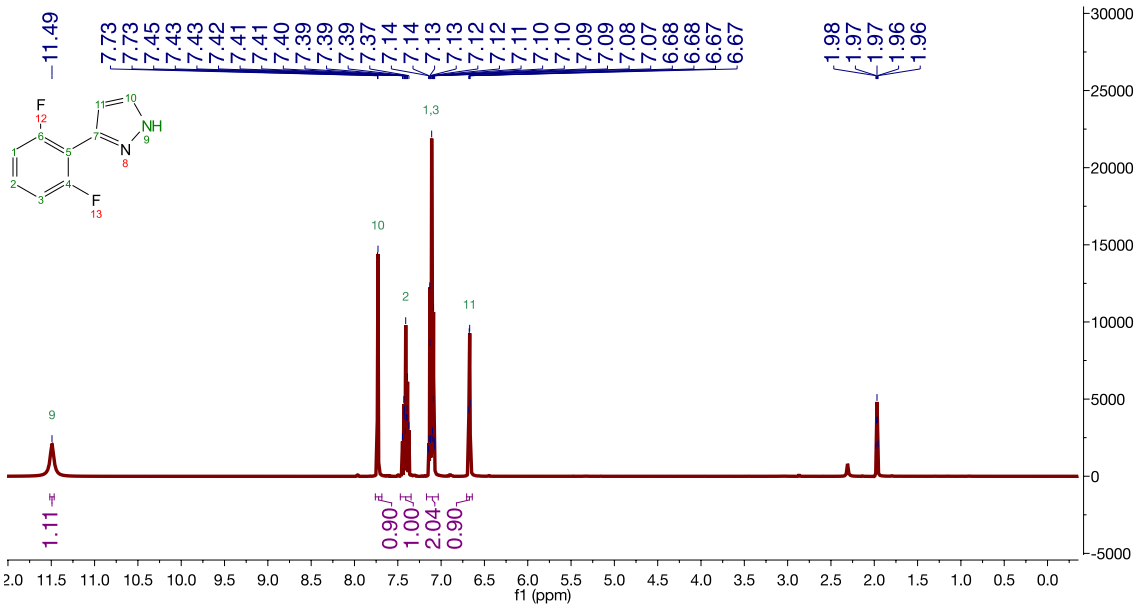

Figure S11. ^{1}H NMR spectrum (400 MHz) of 3-(2,6-difluorophenyl)-1*H*-pyrazole in CD_3CN.

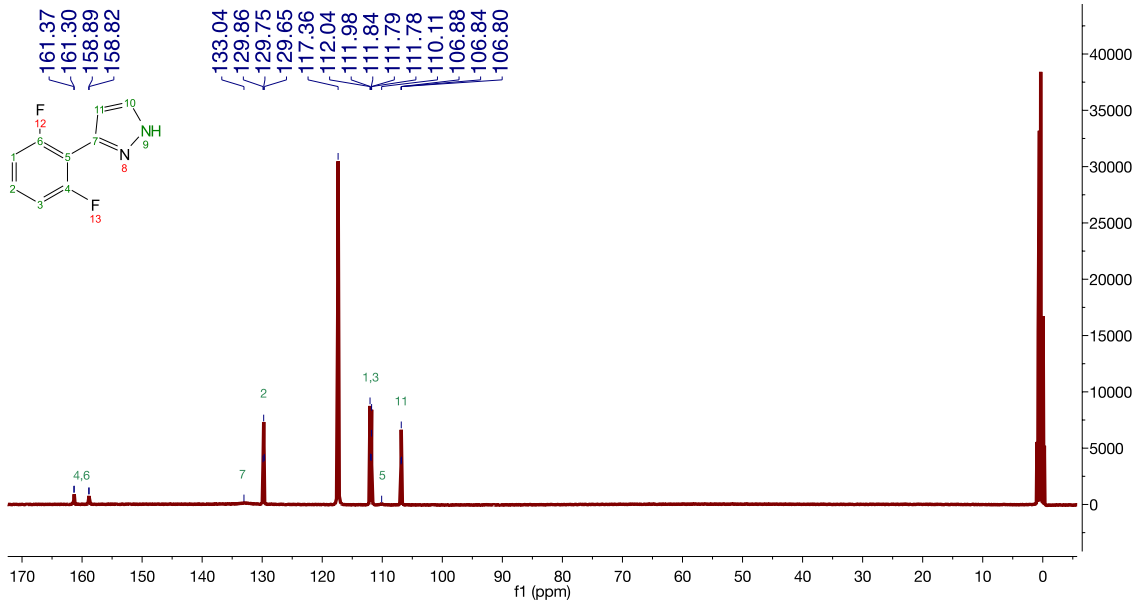

Figure S12. ^{13}C NMR spectrum (400 MHz) of 3-(2,6-difluorophenyl)-1*H*-pyrazole in CD_3CN.

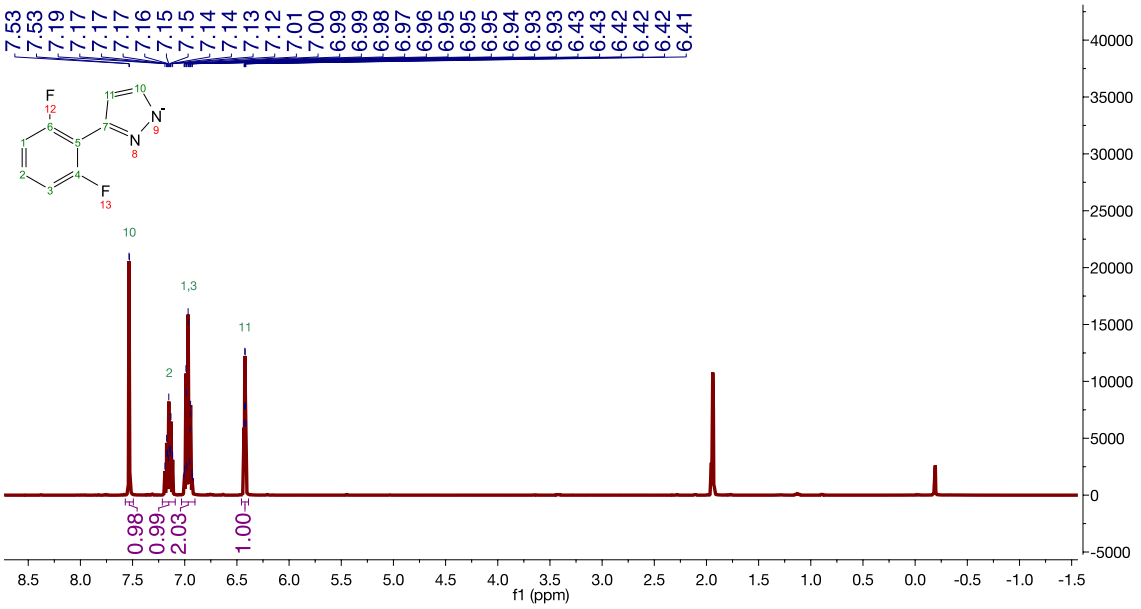

Figure S13. ^{1}H NMR spectrum (400 MHz) of sodium 3-(2,6-difluorophenyl)pyrazolate in CD_3CN.

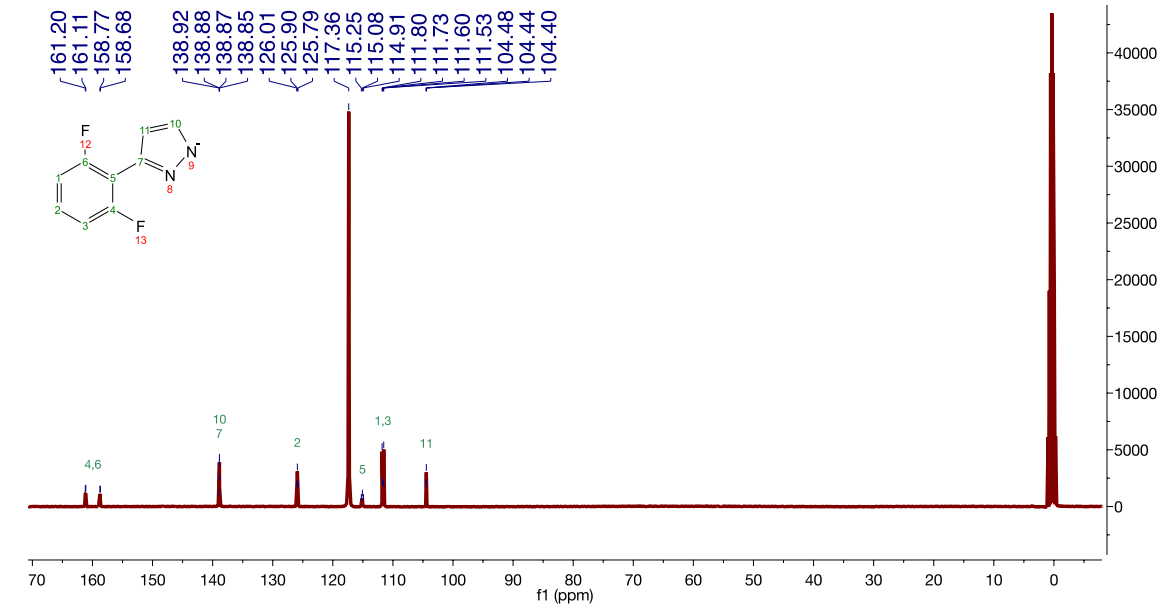

Figure S14. ^{13}C NMR spectrum (400 MHz) of sodium 3-(2,6-difluorophenyl)pyrazolate in CD_3CN.

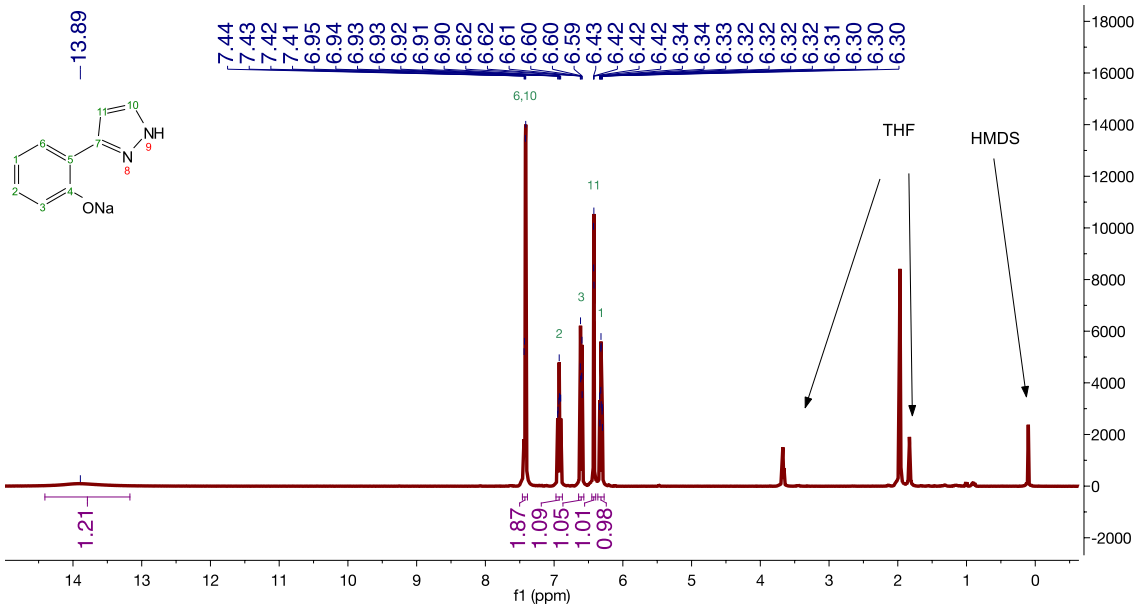

Figure S15. ^{1}H NMR spectrum (400 MHz) of sodium 2-(1H-pyrazol-3-yl)phenolate in CD_3CN.

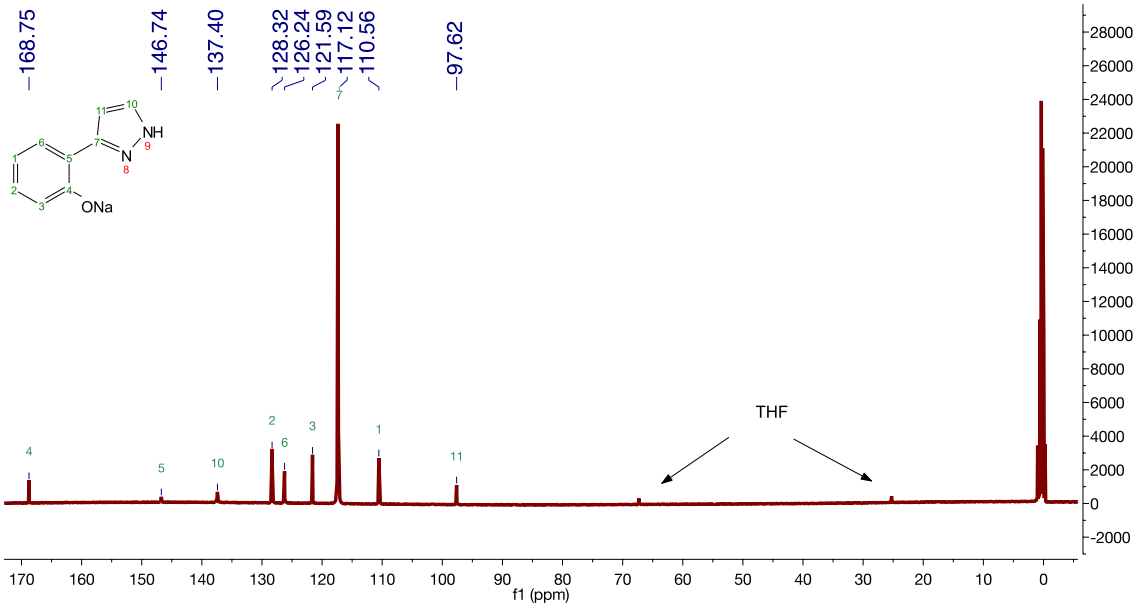

Figure S16. ^{13}C NMR spectrum (400 MHz) of sodium 2-(1H-pyrazol-3-yl)phenolate in CD_3CN

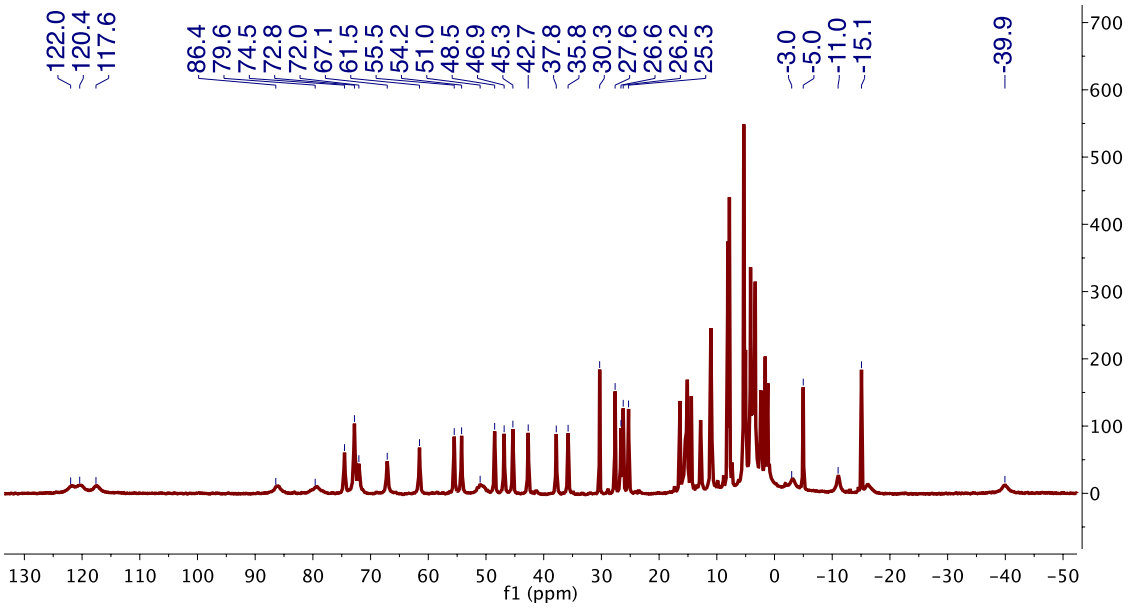

Figure S17. ^{1}H NMR spectrum (300 MHz) of [$LFe_3(PhPz)_2(OArPz)OFe$][OTf] (**3**) in CD_2Cl_2 from method A.

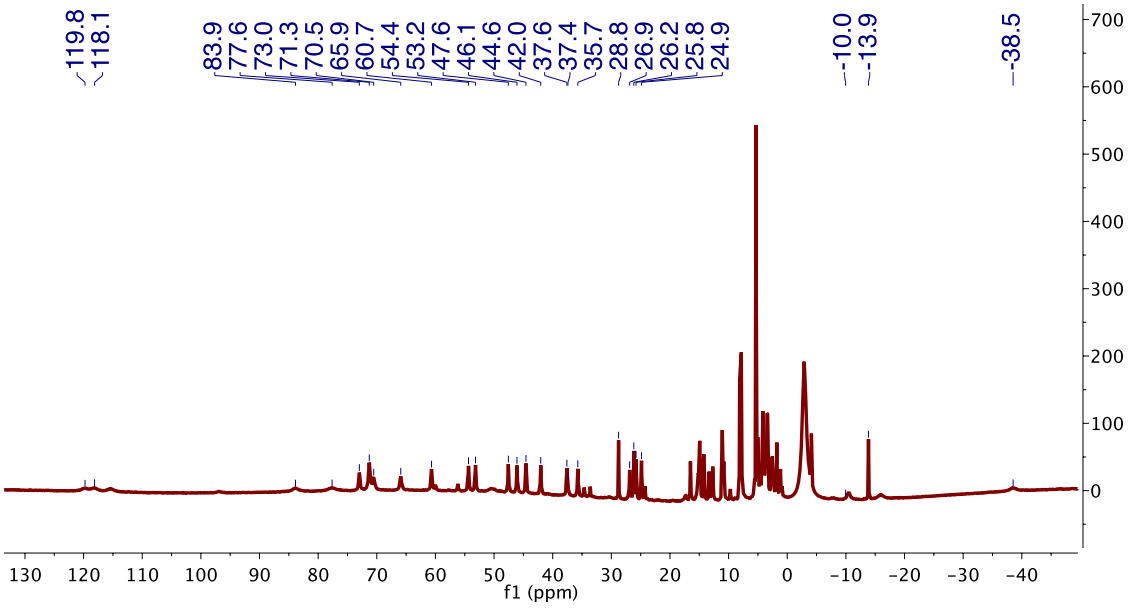

Figure S18. ^{1}H NMR spectrum (300 MHz) of [$LFe_3(PhPz)_2(OArPz)OFe$][OTf] (**3**) in CD_2Cl_2 from method B.

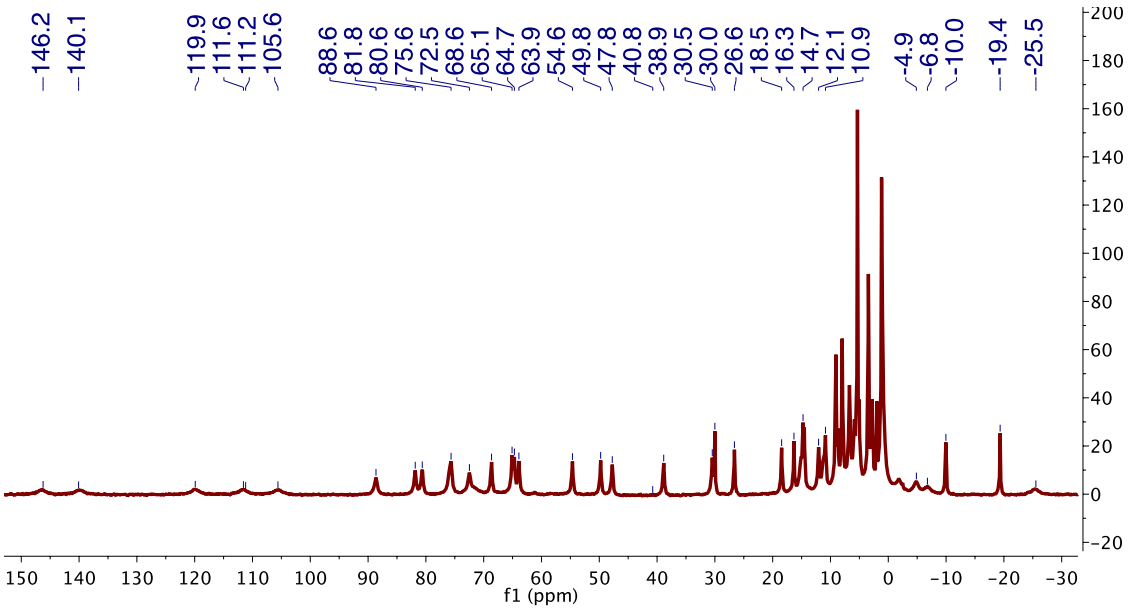

Figure S19. ^{1}H NMR spectrum (300 MHz) of $[LFe_3(PhPz)_2(OArPz)OFe][OTf]_2$ (**2**) in CD_2Cl_2 from method A.

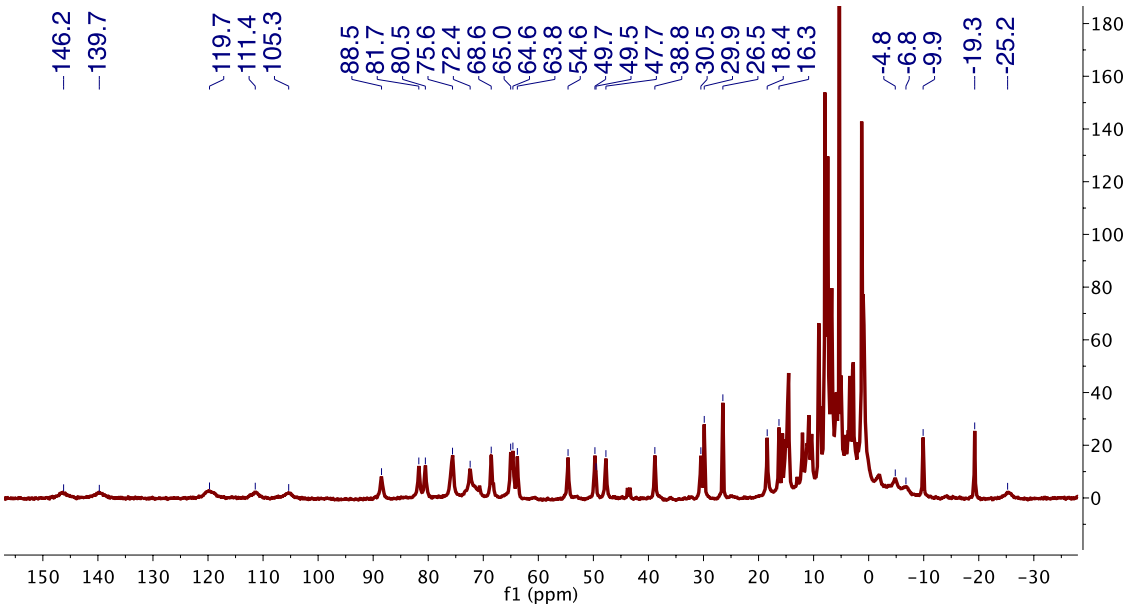

Figure S20. ^{1}H NMR spectrum (300 MHz) of $[LFe_3(PhPz)_2(OArPz)OFe][OTf]_2$ (**2**) in CD_2Cl_2 from method B.

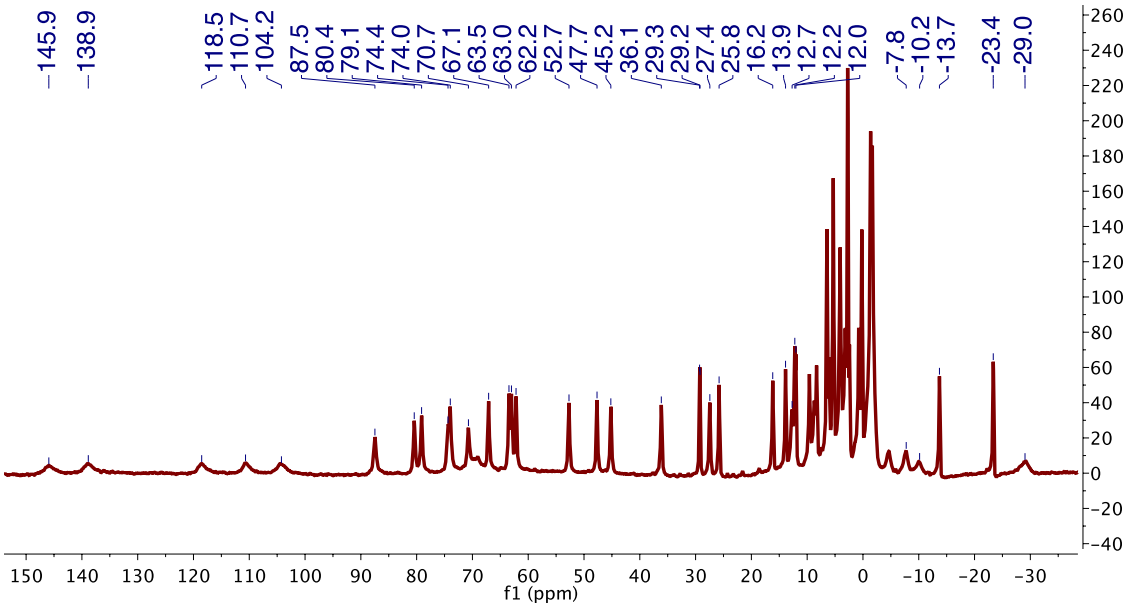

Figure S21. ^{1}H NMR spectrum (300 MHz) of $[LFe_3(PhPz)_2(OArPz)OFe][OTf]_2$ (**2**) in CD_2Cl_2 from method C.

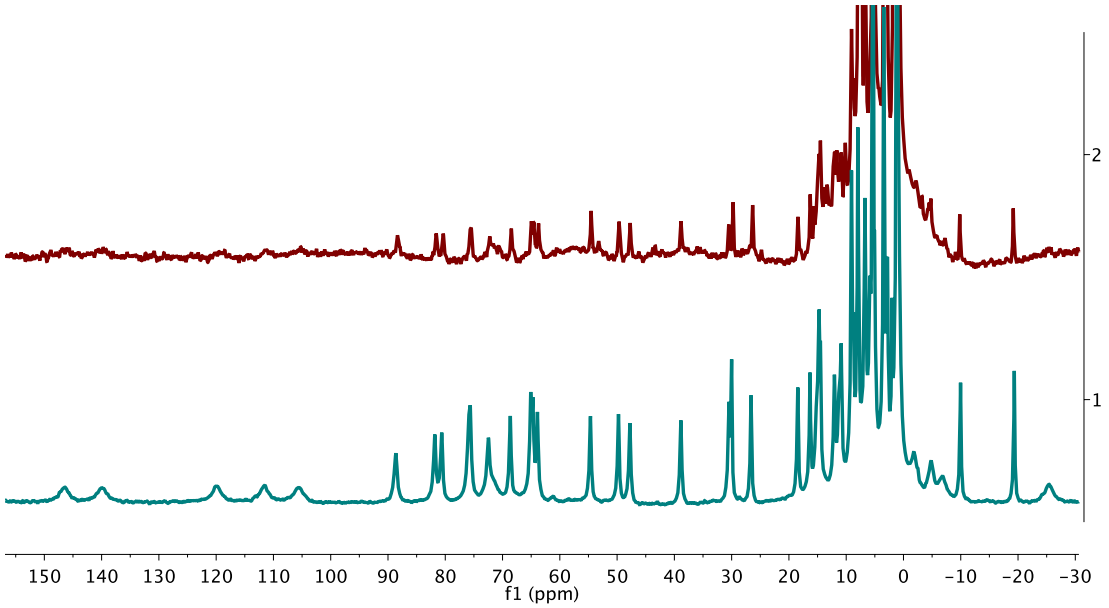

Figure S22. Stacked ^{1}H NMR spectrum (300 MHz) of $[LFe_3(PhPz)_2(OArPz)OFe][OTf]_2$ (**2**) from method D (red), and with $[LFe_3(PhPz)_2(OArPz)OFe][OTf]_2$ (**2**) from method A (green) in CD_2Cl_2.

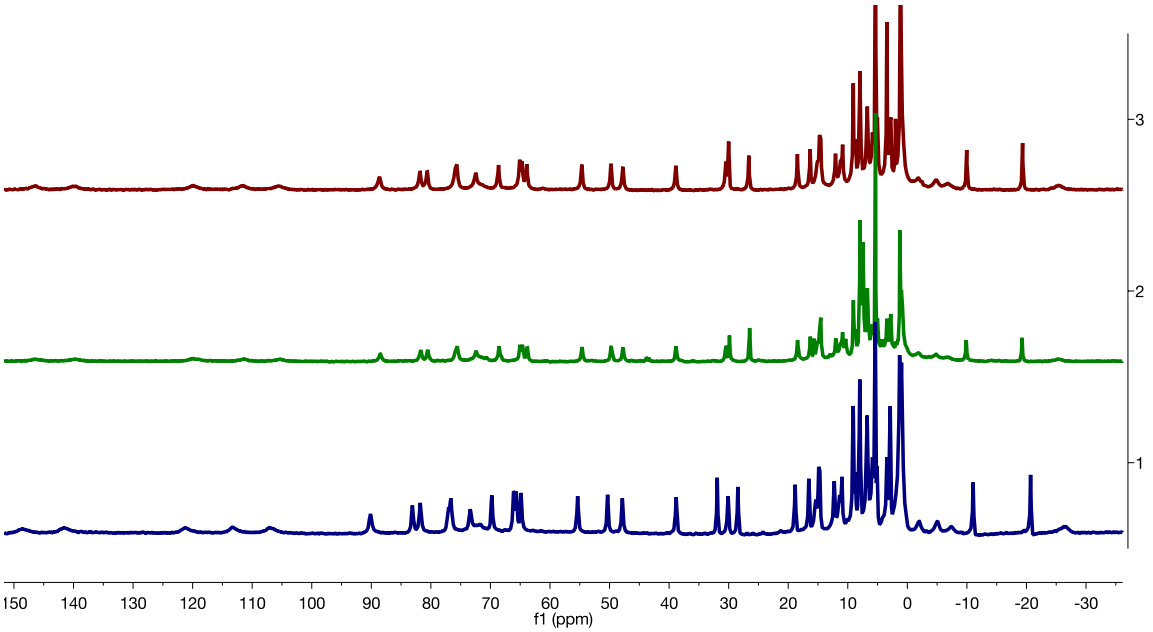

Figure S23. Stacked ^{1}H NMR spectrum (300 MHz) of $[LFe_3(PhPz)_2(OArPz)OFe][OTf]_2$ (**2**) in CD_2Cl_2 from method A–C.

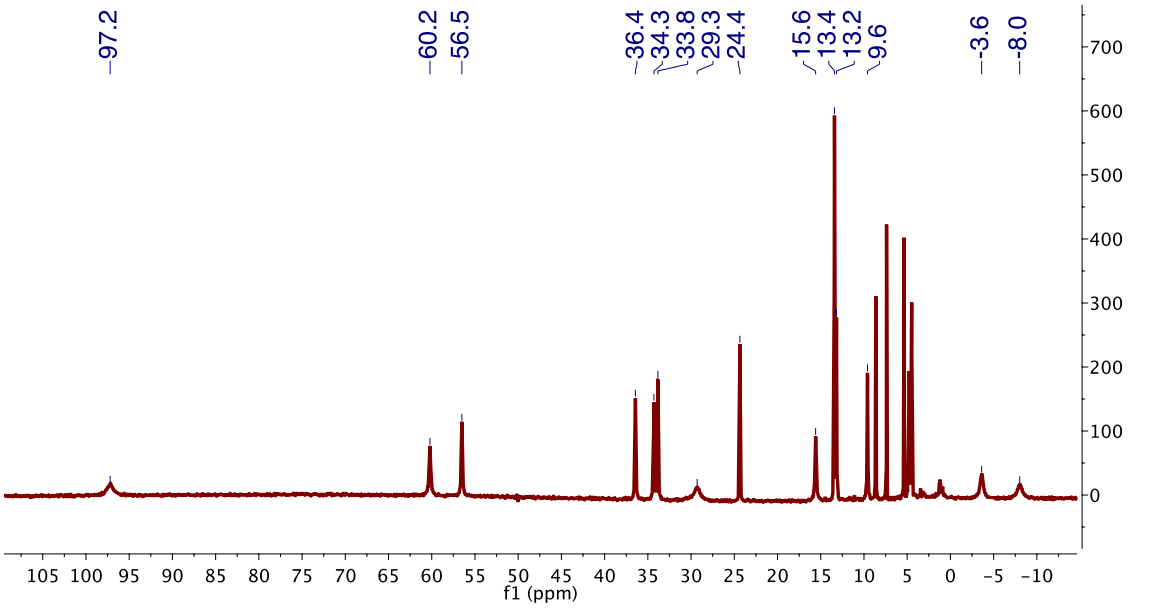

Figure S24. ^{1}H NMR spectrum (300 MHz) of $[LFe_3(F_2ArPz)_3OFe][OTf]$ (**4**) in CD_2Cl_2.

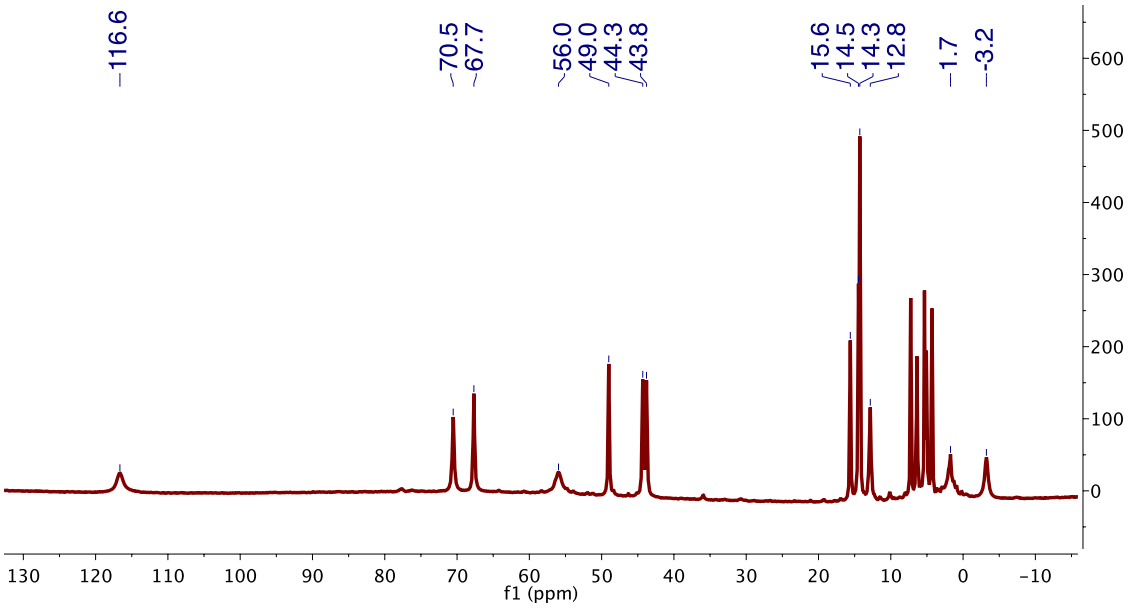

Figure S25. ^{1}H NMR spectrum (300 MHz) of $[LFe_3(F_2arPz)_3OFe][OTf]_2$ (**5**) in CD_2Cl_2.

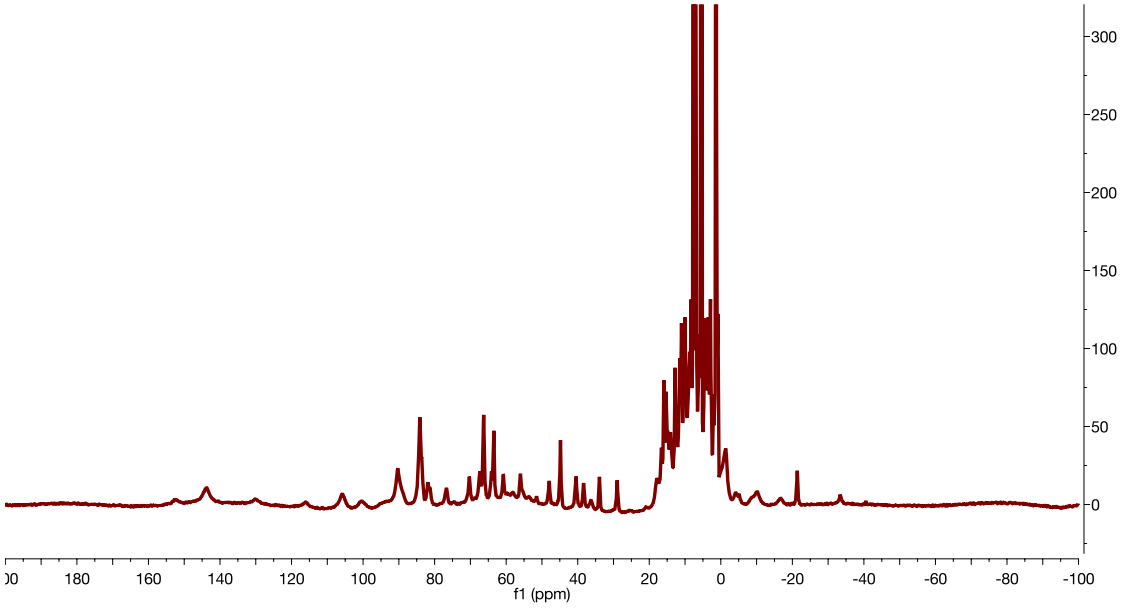

Figure S26. Crude ^{1}H NMR spectrum (300 MHz) of the reaction of $[LFe_3(F_2ArPz)_3OFe][OTf]_2$ (**5**) with PhIO for 16 h. in CD_2Cl_2.

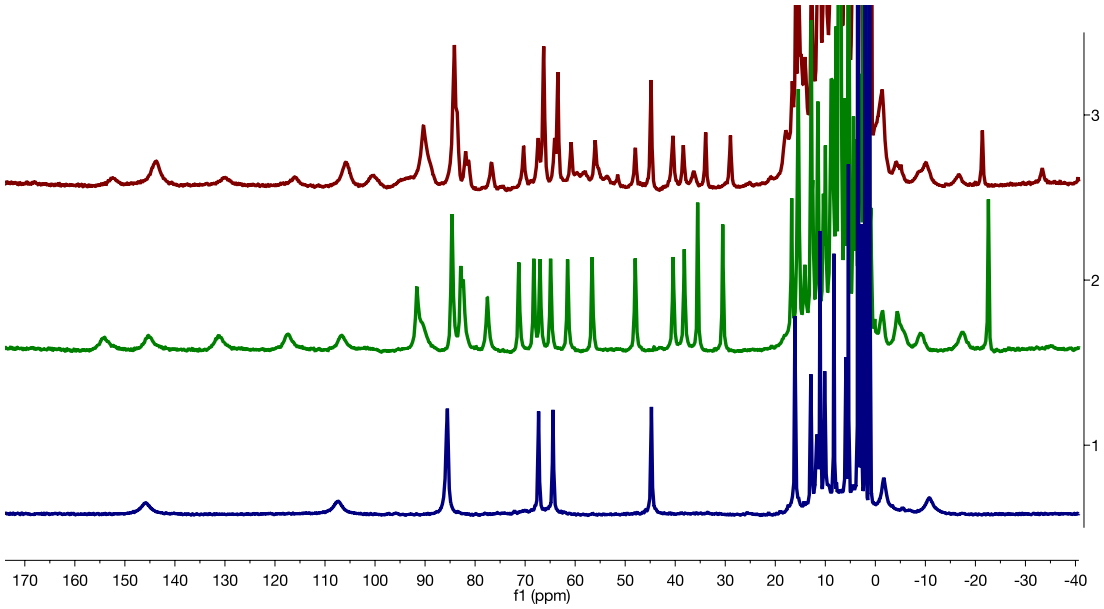

Figure S27. Stacked ^{1}H NMR spectrum (300 MHz) of $[LFe_3(F_2ArPz)_3OFe][OTf]_2$ (**5**) with PhIO (red), $[LFe_3(F_2ArPz)_2(OFArPz)OFe][OTf]_2$ (**7**; green), and $[LFe_3(F_2ArPz)_3OFe(F)][OTf]_2$ (**8**); blue) in CD_2Cl_2.

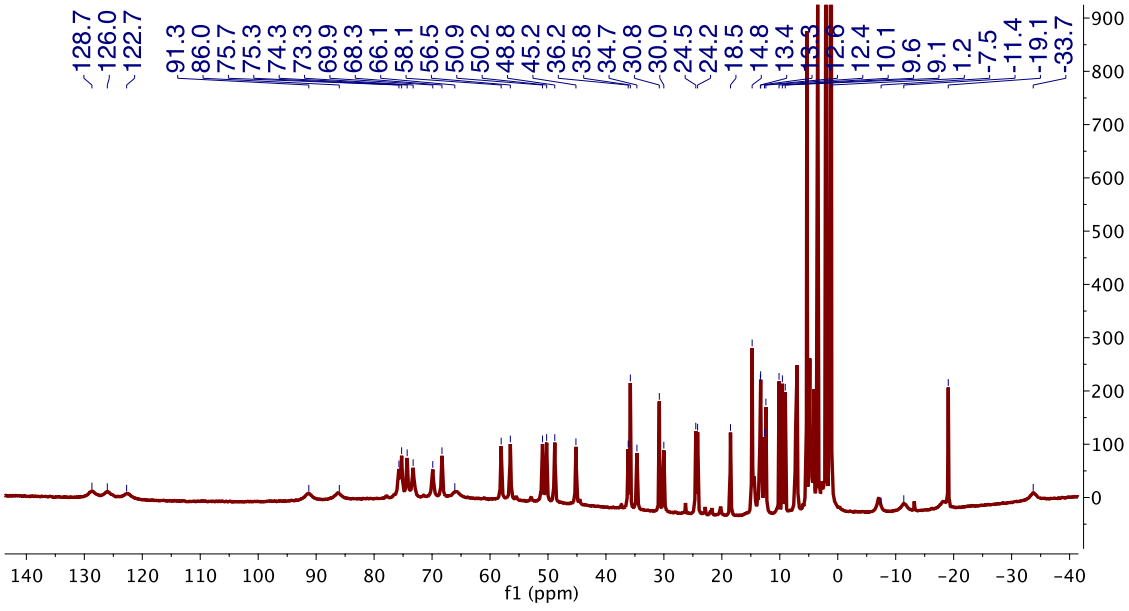

Figure S28. ^{1}H NMR spectrum (300 MHz) of $[LFe_3(F_2ArPz)_2(OFArPz)OFe][OTf]$ (**6**) in CD_2Cl_2.

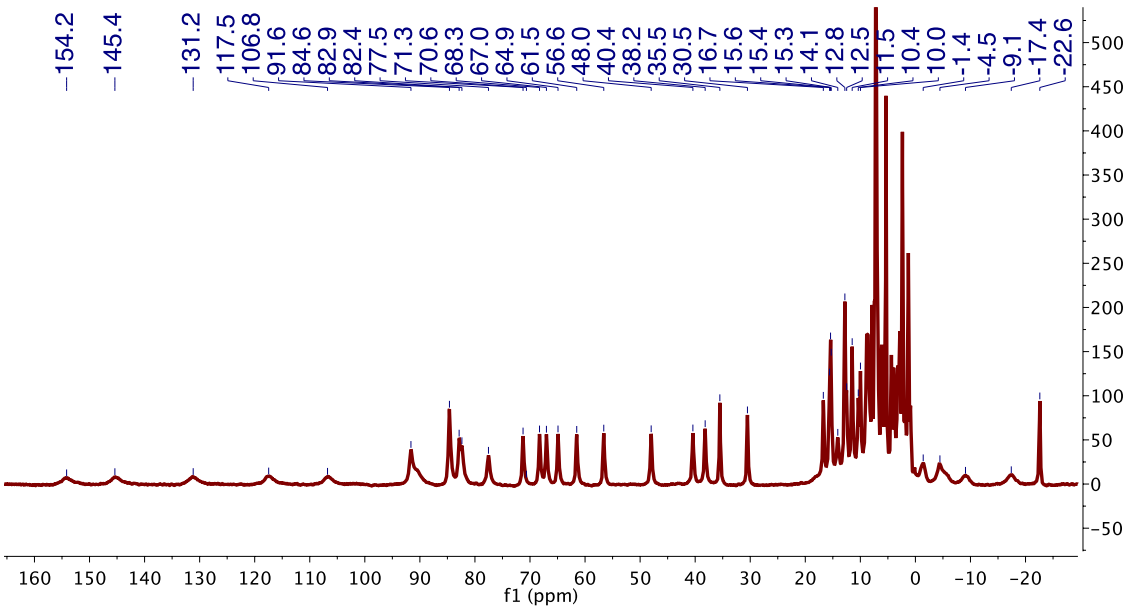

Figure S29. ^{1}H NMR spectrum (300 MHz) of [$LFe_3(F_2ArPz)_2(OFArPz)OFe$][$OTf]_2$ (**7**) in CD_2Cl_2 from method A.

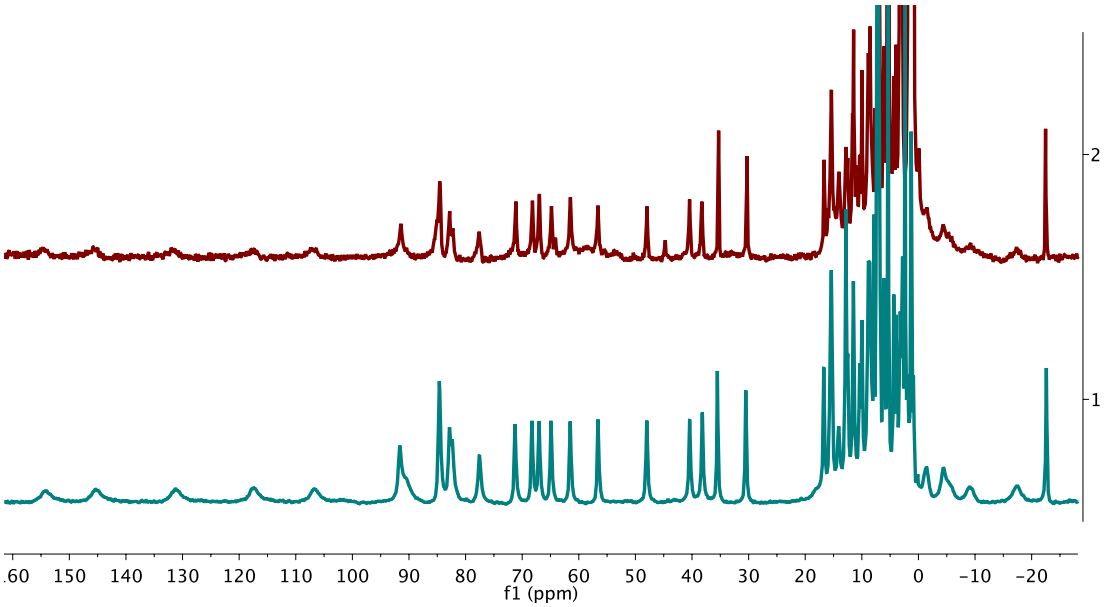

Figure S30. Stacked ^{1}H NMR spectrum (300 MHz) of [$LFe_3(F_2ArPz)_2(OFArPz)OFe$][$OTf]_2$ (**7**) from method B (red), and with [$LFe_3(F_2ArPz)_2(OFArPz)OFe$][$OTf]_2$ (**7**) from method A (green) in CD_2Cl_2.

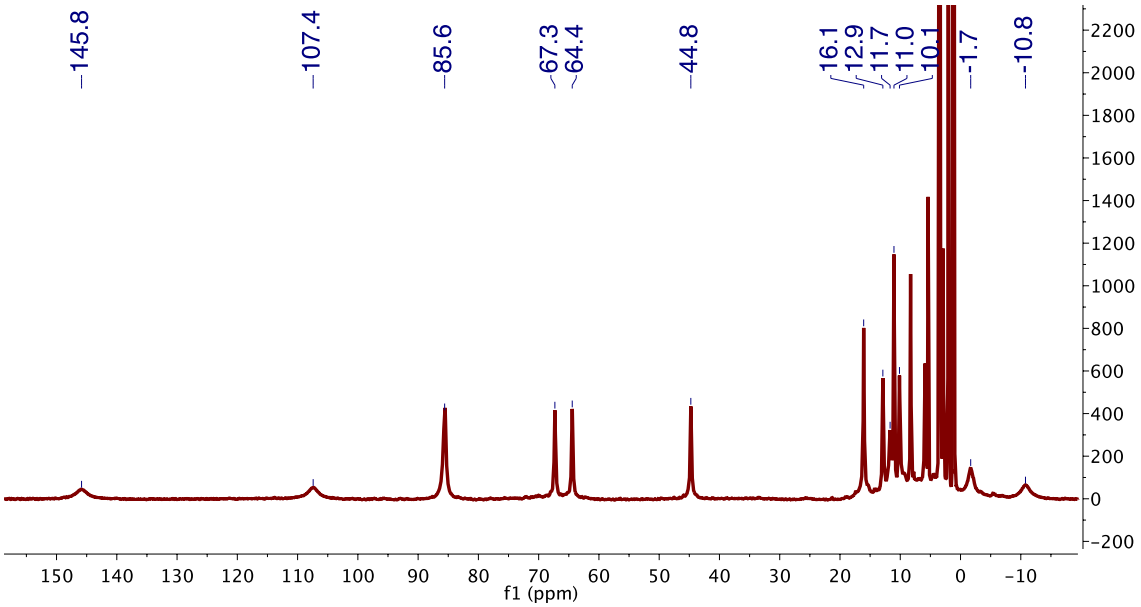

Figure S31. ^{1}H NMR spectrum (300 MHz) of $[LFe_3(F_2ArPz)_3OFe(F)][OTf]_2$ (**8**) in CD_2Cl_2.

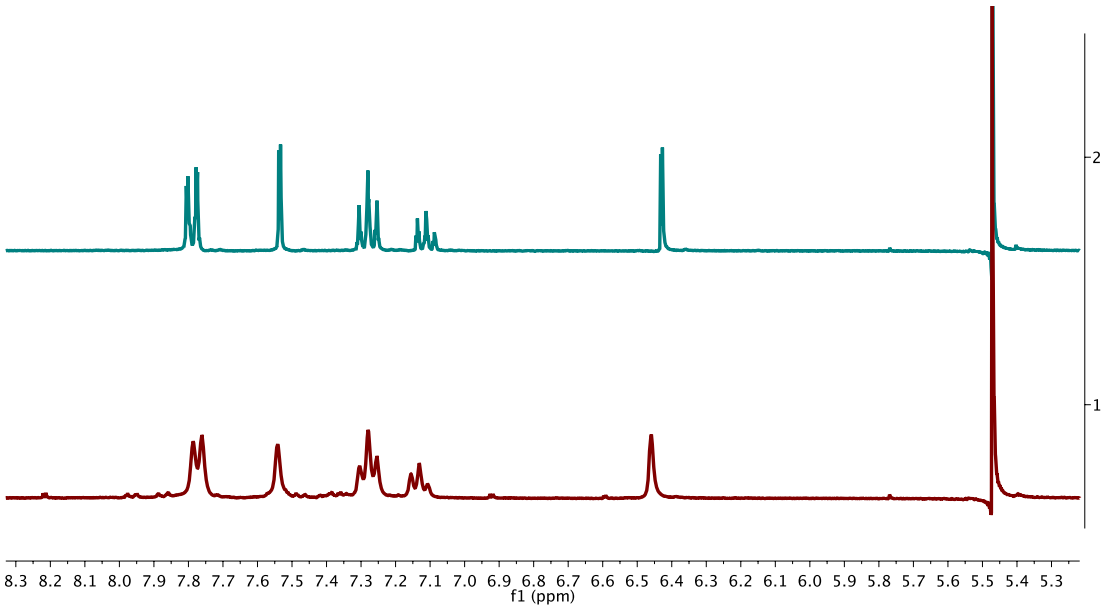

Figure S32. ^{1}H NMR spectrum (300 MHz) of NaPhPz in CD_3CN (top), and that of the crude reaction mixture upon reacting NaPhPz with PhIO (bottom).

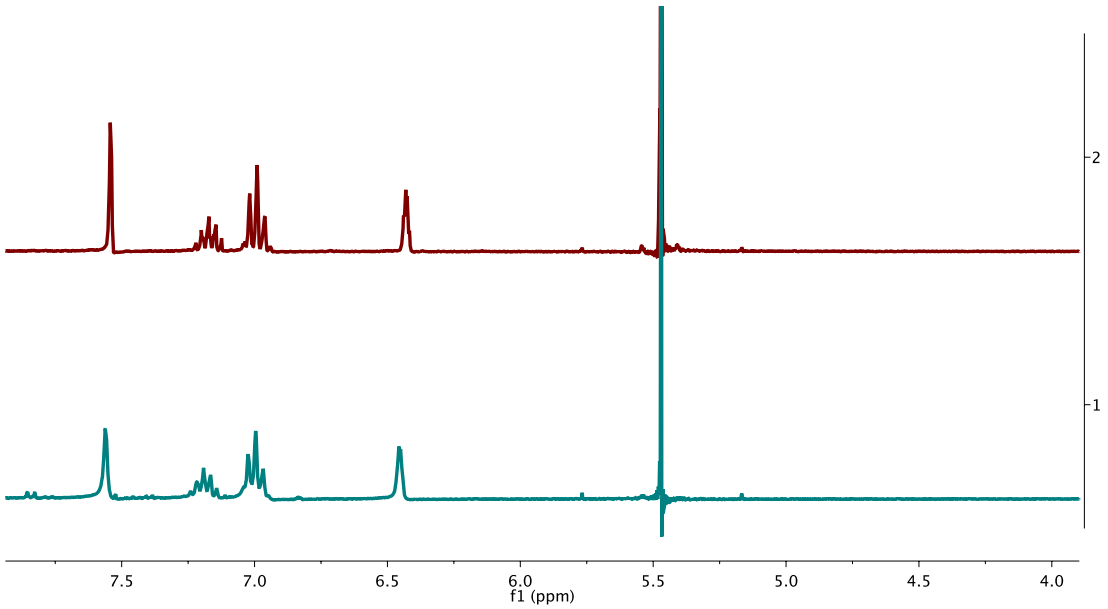

Figure S33. ^{1}H NMR spectrum (300 MHz) of NaF_2ArPz in CD_3CN (top), and that of the crude reaction mixture upon reacting NaF_2ArPz with PhIO (bottom).

A)

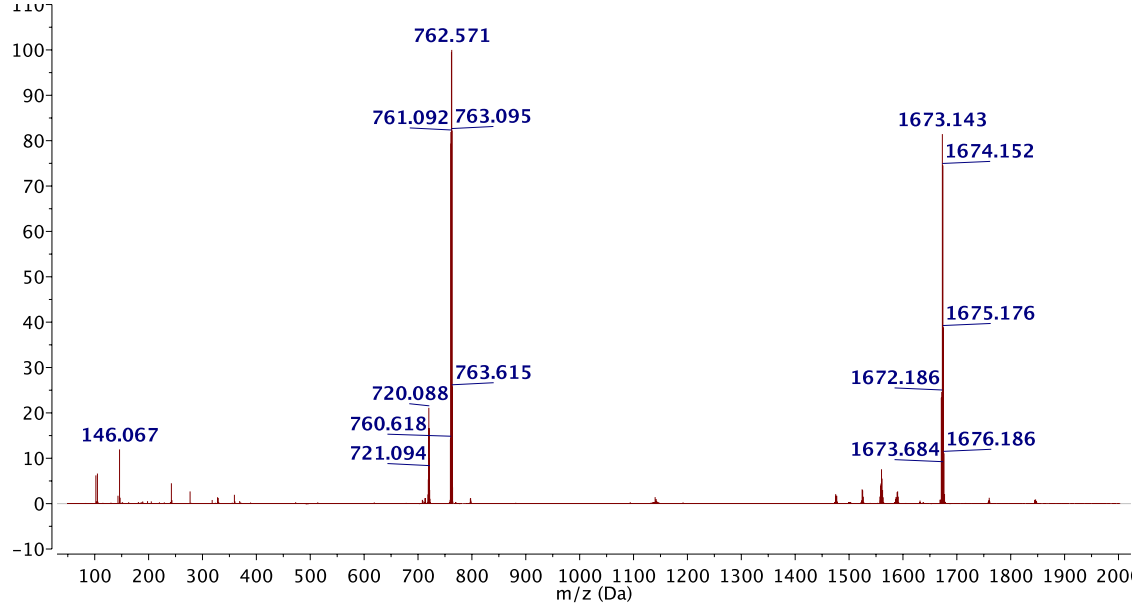

B)

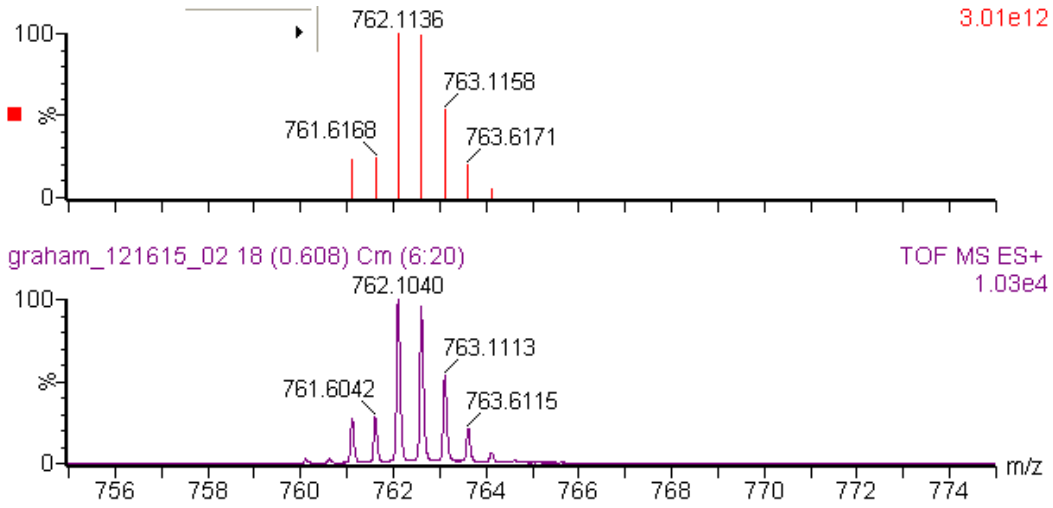

Figure S34. Electrospray Ionization Mass spectrum (ESI-MS) of (A) the crude reaction mixture upon treatment of **2** with PhIO and (B) the corresponding isotope distribution pattern.

A)

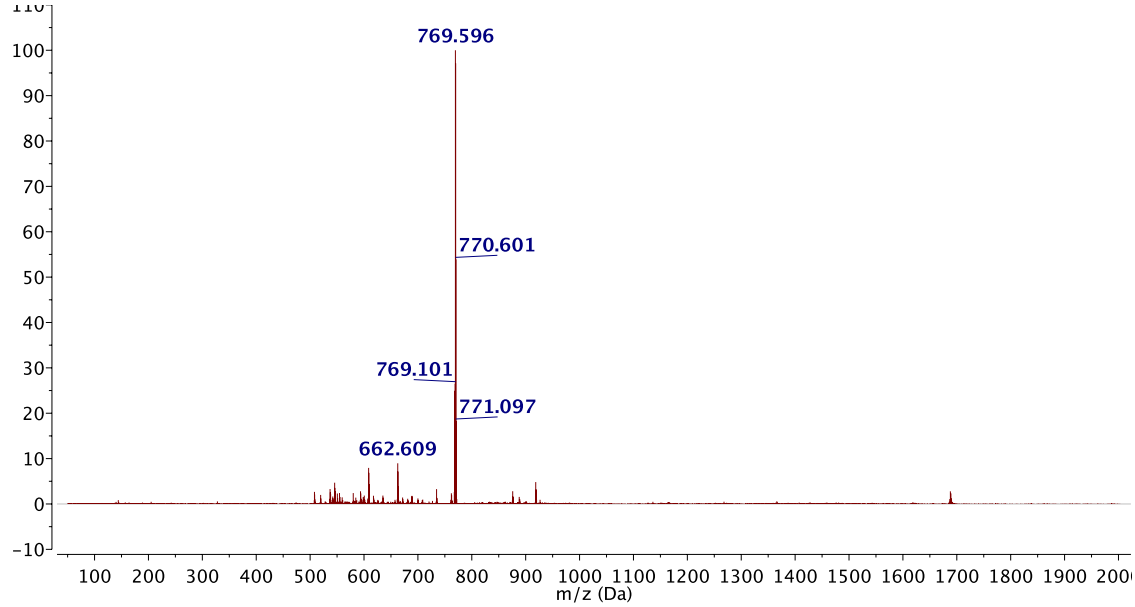

B)

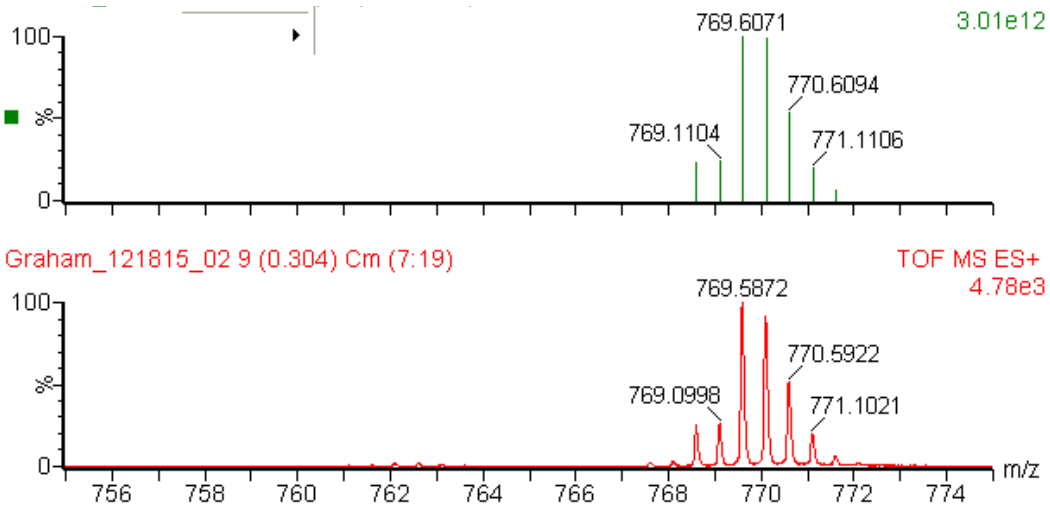

Figure S35. Electrospray Ionization Mass spectrum (ESI-MS) of (A) the crude reaction mixture upon treatment of **2** with PhIO and (B) the corresponding isotope distribution pattern.

A)

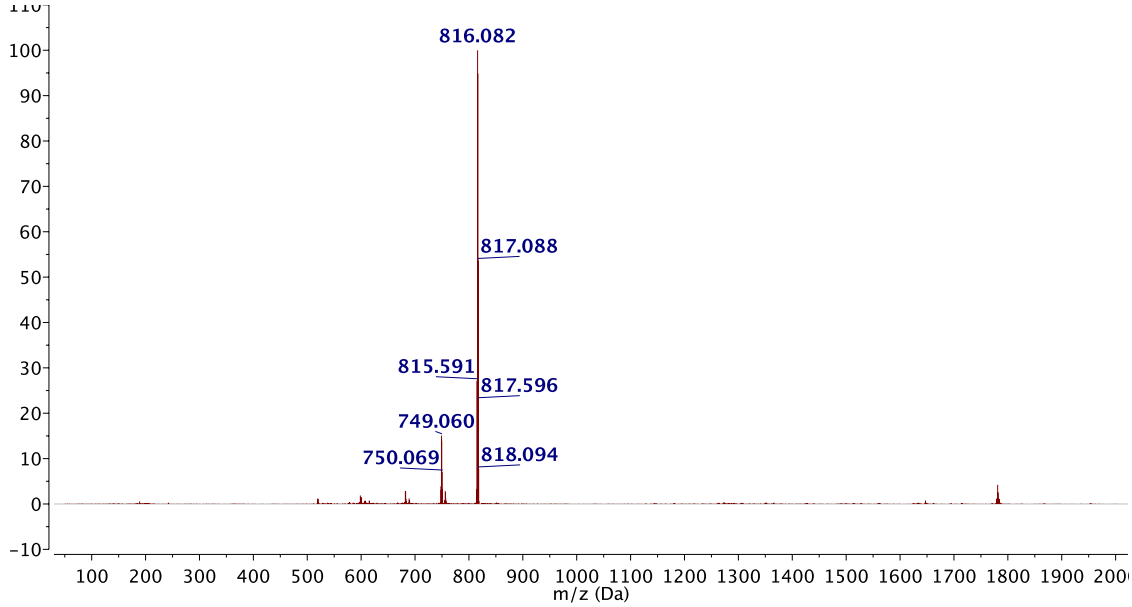

B)

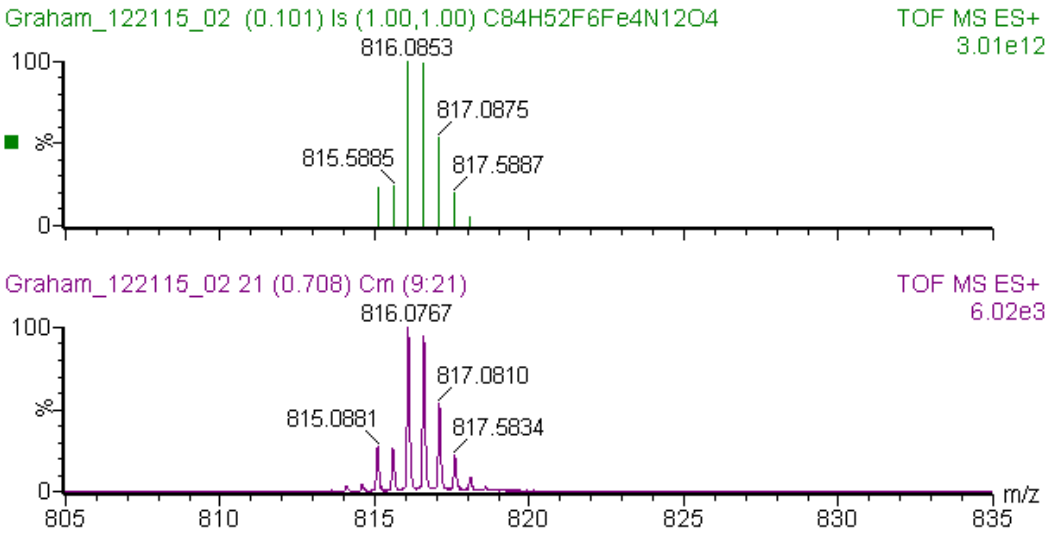

Figure S36. Electrospray Ionization Mass spectrum (ESI-MS) of (A) $[LFe_3(F_2ArPz)_3OFe][OTf]_2$ (**5**) and (B) the corresponding isotope distribution pattern.

A)

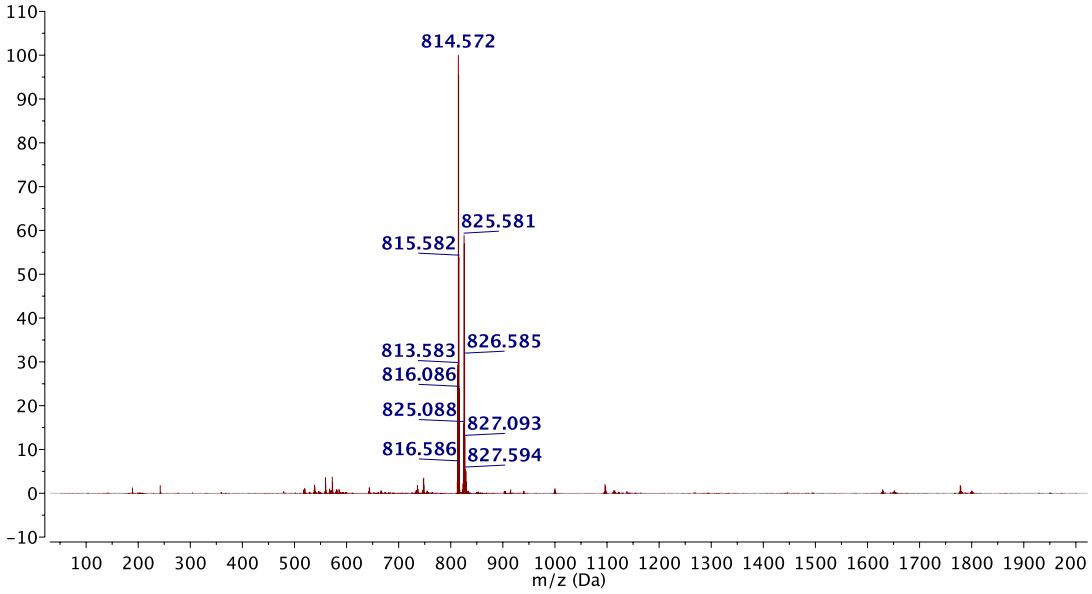

B)

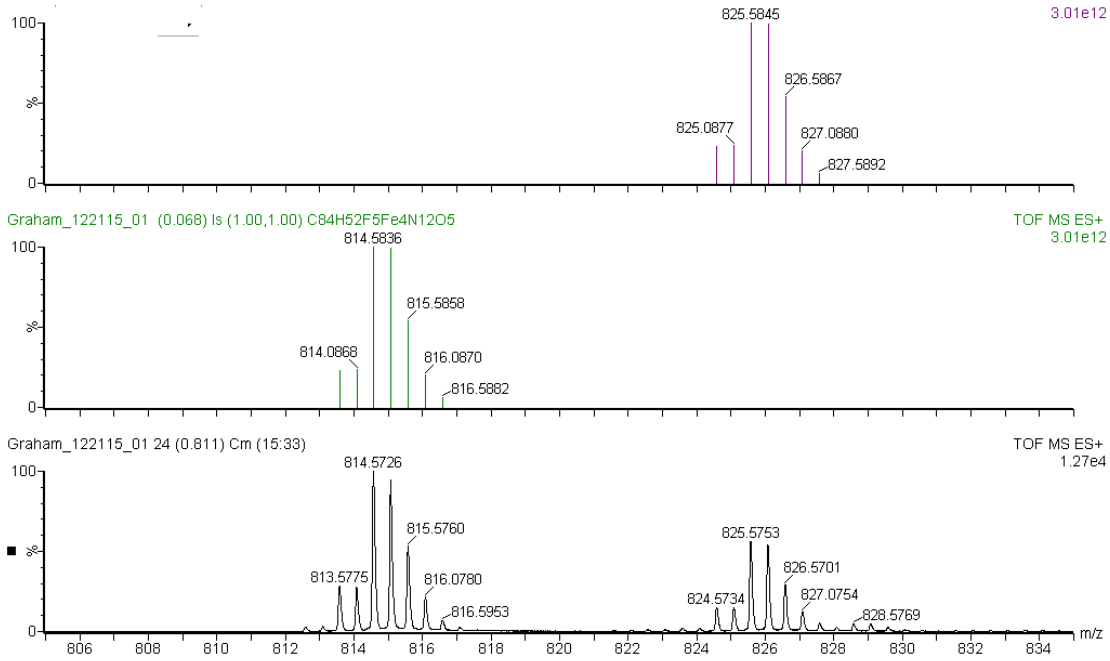

Figure S37. Electrospray Ionization Mass spectrum (ESI-MS) of (A) the crude reaction mixture upon treatment of **5** with PhIO and (B) the corresponding isotope distribution pattern.

Mössbauer simulation details for compounds 2, 3, and 5-8. All spectra were simulated by four pairs of symmetric quadrupole doublets with equal populations and Lorentzian lineshapes, and refined to a minimum by the method of least squares optimization (a total of 13 fitting parameters per spectrum). For all spectra, the observed resonances spanned the region from -1–3 mm s^{-1}. Any resonances appearing above 2 mm s^{-1} indicate the presence of high spin Fe(II) centers and must correspond to species with isomer shifts ~1 mm s^{-1}, given the range of observed resonances. Details regarding the fitting of individual spectra are given below. In short, the Mössbauer data were modeled to be consistent with our previously reported triiron-oxo/hydroxyl clusters,[8] and our previously reported tetranuclear iron clusters.[2] Overall, the observed Mössbauer parameters are in-line with those of other six-coordinate FeII/FeIII centers bearing N- and O-donor atoms.[9-16]

Simulation details for $[LFe_3(PhPz)_2(OPhPz)OFe][OTf]_2$ (2): The Mössbauer spectrum of **2** features only five well-resolved resonances (opposed to the expected 8). A single symmetric Lorentzian appearing around 3 mm/s suggests a single high spin Fe(II) center, which is consistent with the crystallographic analysis of the basal Fe_3 core (*vide infra*). The residual signals are centered on 0.5 mm/s, and within the range expected for high spin Fe(III) ions. An initial simulation was performed using only three quadrupole doublets to fit the five observed features (Fig. S38A). After optimization, the refined parameters were consistent with two high spin Fe(III) and one high spin Fe(II) in a 2:1:1 ratio. Thus, to obtain a final simulation, the most intense Fe(III) signal was split into two distinct resonances, and all species were refined with equal populations (Fig. S38B).

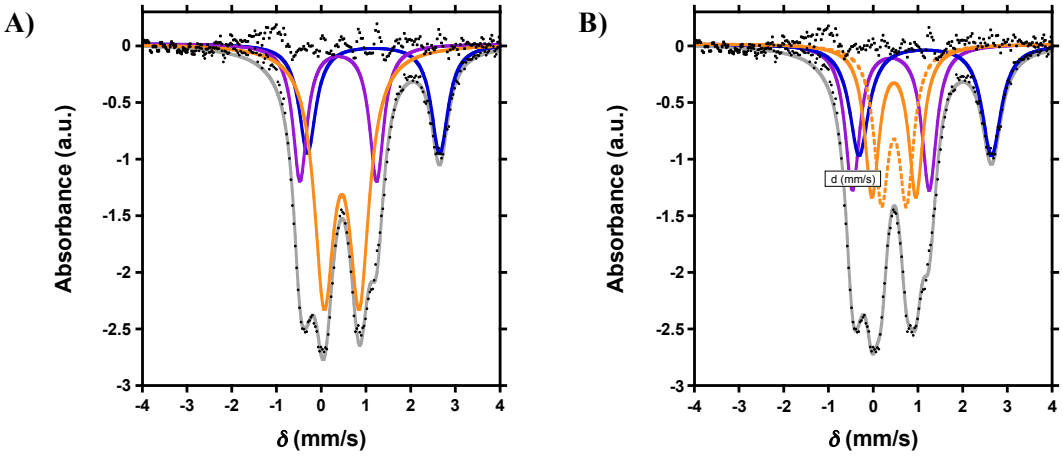

Figure S38. (A) Initial simulation of **2** (black dots) fit to three quadrupole doublets. Simulation is shown in grey, with parameters: (i) δ = 1.17 mm/s, $|\Delta E_Q|$ = 2.96 mm/s (23%, solid blue trace); (ii) δ = 0.38 mm/s, $|\Delta E_Q|$ = 1.72 mm/s (24%, purple red trace); and (iii) δ = 0.46 mm/s, $|\Delta E_Q|$ =

0.79 mm/s (59%, solid orange trace). Residuals shown in black (SSE = 1.42). (B) Final simulation of **2** (black dots) fit to four quadrupole doublets. Simulation is shown in grey, with parameters: (i) δ = 1.17 mm/s, $|\Delta E_Q|$ = 2.96 mm/s (26%, solid blue trace); (ii) δ = 0.40 mm/s, $|\Delta E_Q|$ = 1.72 mm/s (26%, solid purple trace); (iii) δ = 0.47 mm/s, $|\Delta E_Q|$ = 0.99 mm/s (26%, dashed orange trace); and (iv) δ = 0.47 mm/s, $|\Delta E_Q|$ = 0.56 mm/s (26%, solid orange trace). Residuals shown in black (SSE = 1.27).

Simulation details for [LFe$_3$(PhPz)$_2$(OPhPz)OFe][OTf] (3): The Mössbauer spectrum of **3** exhibits five well-resolved resonances. As with **2**, the Lorentzian appearing near 3 mm/s suggests the presence of high spin ferrous ions, and the asymmetric line shape further indicates at least two such Fe(II) centers, which is consistent with the crystallographic analysis of the basal Fe$_3$ core (*vide infra*). Based on the positions and intensities of the nearly overlapping Fe(II) quadrupole doublets, these features can be straightforwardly modeled and subtracted to clarify further analysis (Fig. S39A–B). After subtraction, the residual signal reveals four Lorentzians of approximately equal area, and thus *a priori* there are three reasonable simulations. As one simulation leads to a quadrupole doublet with a negative isomer shift, this simulation was rejected (not shown). Of the remaining two simulations of the Fe(III) metal centers, the one shown in Figure S39B (orange and purple traces) provides a superior fit to the data, and also reveals Mössbauer parameters typical of high spin Fe(III) centers. Moreover, the observed isomer shifts match well with those found for the Fe(III) centers of **2** (vide supra). Thus the final simulation shown in Figure S39B is preferred to that shown in Figure 39A. Consequently, the final simulation shown in Figure S39D is preferred to that shown in C.

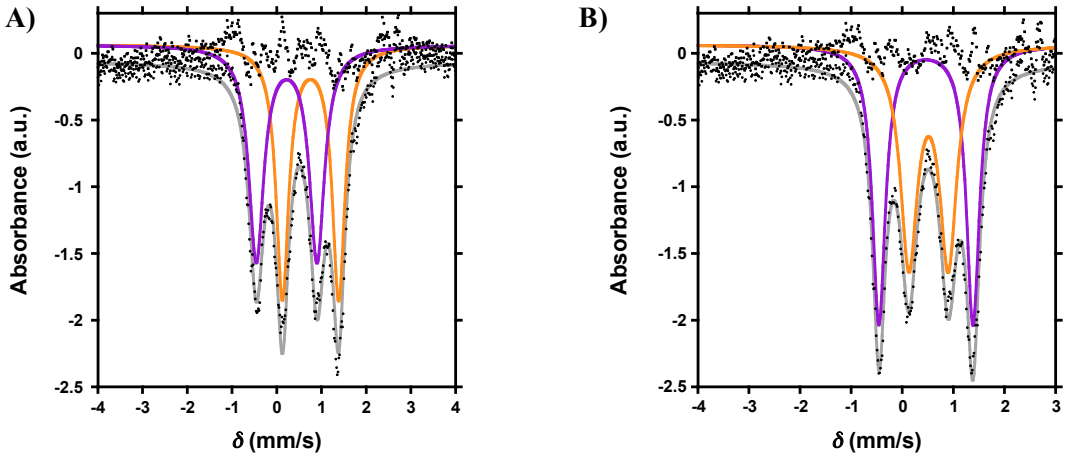

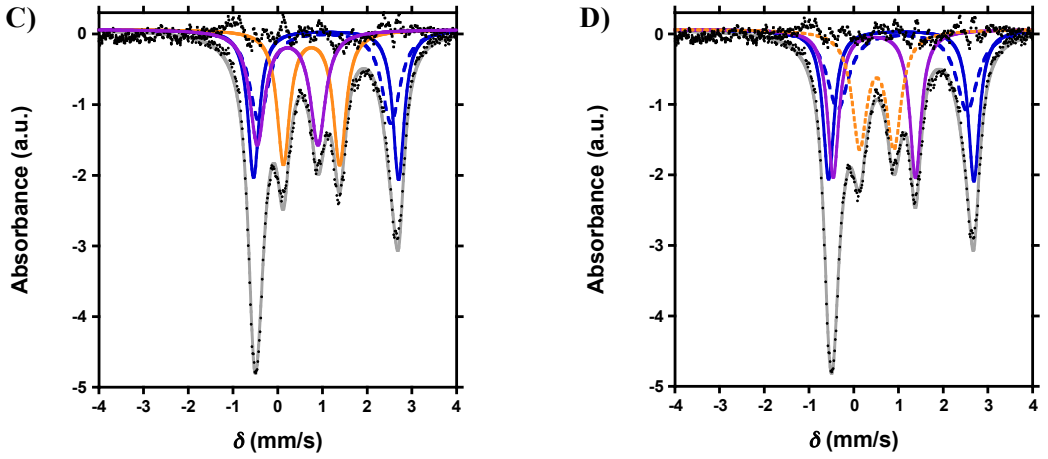

Figure S39. (A) Simulation of **3** (black dots) after subtraction of high spin Fe(II) components. Simulation is shown in grey, with parameters: (i) δ = 0.76 mm/s, $|\Delta E_Q|$ = 1.26 mm/s (solid orange trace); and (ii) δ = 0.22 mm/s, $|\Delta E_Q|$ = 1.36 mm/s (solid purple trace). (B) Simulation of **3** (black dots) after subtraction of high spin Fe(II) components. Simulation is shown in grey, with parameters: (i) δ = 0.52 mm/s, $|\Delta E_Q|$ = 0.77 mm/s (solid orange trace); and (ii) δ = 0.46 mm/s, $|\Delta E_Q|$ = 1.84 mm/s (solid purple trace). (C) Simulation of **3** (black dots) fit to four quadrupole doublets. Simulation is shown in grey, with parameters: (i) δ = 1.08 mm/s, $|\Delta E_Q|$ = 3.24 mm/s (solid blue trace); (ii) δ = 1.06 mm/s, $|\Delta E_Q|$ = 2.95 mm/s (dashed blue trace); (iii) δ = 0.76 mm/s, $|\Delta E_Q|$ = 1.26 mm/s (solid orange trace); and (iv) δ = 0.22 mm/s, $|\Delta E_Q|$ = 1.36 mm/s (solid purple trace). (D) Simulation of **3** (black dots) fit to four quadrupole doublets. Simulation is shown in grey, with parameters: (i) δ = 1.08 mm/s, $|\Delta E_Q|$ = 3.24 mm/s (solid blue trace); and (ii) δ = 1.06 mm/s, $|\Delta E_Q|$ = 2.95 mm/s (dashed blue trace) (iii) δ = 0.52 mm/s, $|\Delta E_Q|$ = 0.77 mm/s (dashed orange trace); (iv) δ = 0.46 mm/s, $|\Delta E_Q|$ = 1.84 mm/s (solid purple trace). Residuals are shown in black (SSE = 4.57 for A and = 3.61 for B).

Simulation details for $[LFe_3(F_2ArPz)_3OFe][OTf]_2$ (5): The Mössbauer spectrum of **5** exhibits five resolved features, with the Lorentzians appearing near 3 mm s^{-1} indicating the presence of two high spin ferrous ions. The spectrum was preliminarily simulated with a set of three quadrupole doublets to fit the five features, resulting in two reasonable simulations (Fig. S40A–B). Both simulations result in parameters consistent with two high spin Fe(II) centers and a high spin Fe(III) center in a 1:1:2 ratio. The spectrum shown in Figure S40B furnishes a slightly superior simulation, and has parameters for the Fe(II) ions that are self-consistent with those observed for the other species reported here, and thus the final simulation was performed by

splitting the Fe(III) resonance in this spectrum in two and refining all species with equal populations (Fig. S40C).

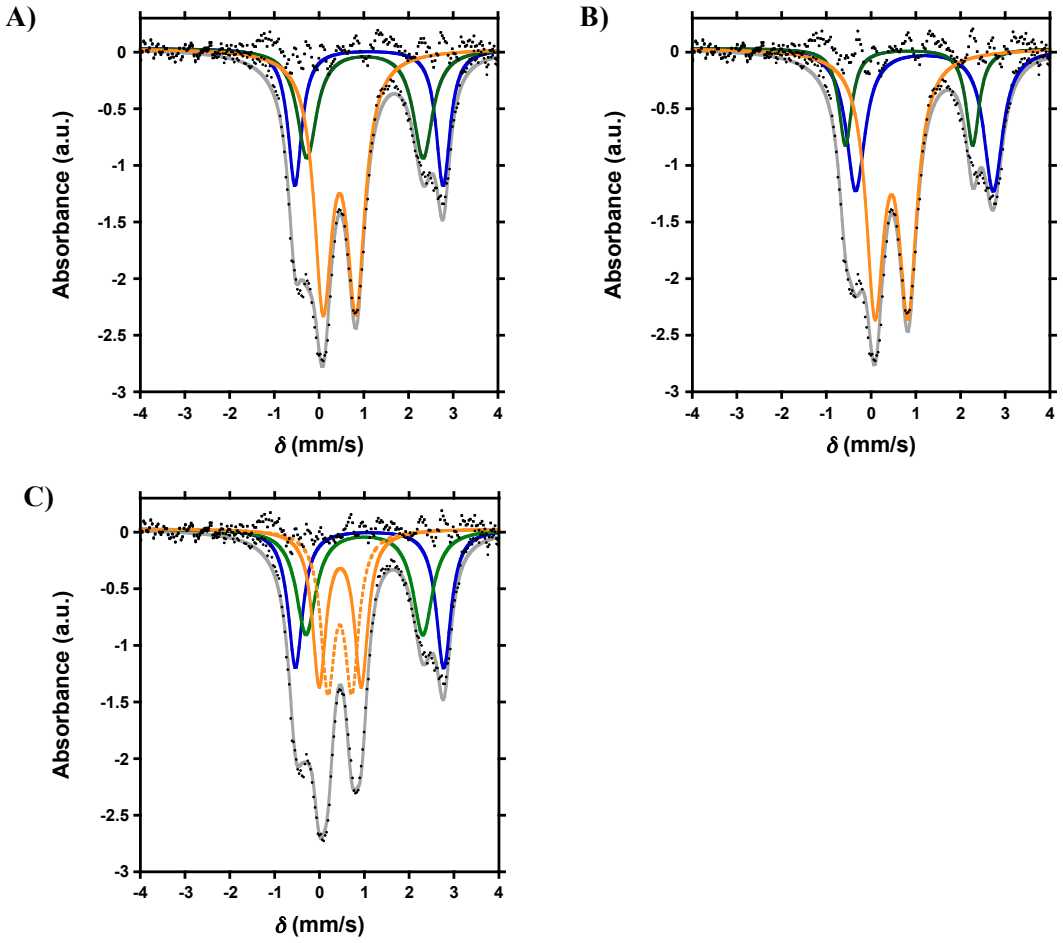

Figure S40. (A) Initial simulation of **5** (black dots) with three quadrupole doublets. Simulation is shown in grey, with parameters: (i) δ = 1.20 mm/s, $|\Delta E_Q|$ = 3.08 mm/s (solid blue trace, 35%); (ii) δ = 0.85 mm/s, $|\Delta E_Q|$ = 2.85 mm/s (solid green trace, 17%); and (iii) δ = 0.46 mm/s, $|\Delta E_Q|$ = 0.74 mm/s (solid orange trace, 58%). (B) Initial simulation of **5** (black dots) with three quadrupole doublets. Simulation is shown in grey, with parameters: (i) δ = 1.12 mm/s, $|\Delta E_Q|$ = 3.32 mm/s (solid blue trace, 25%); (ii) δ = 1.03 mm/s, $|\Delta E_Q|$ = 2.60 mm/s (solid green trace, 28%); and (iii) δ = 0.46 mm/s, $|\Delta E_Q|$ = 0.74 mm/s (solid orange trace, 58%). (C) Final simulation of **5** (black dots) with four quadrupole doublets. Simulation is shown in red, with parameters: (i) δ = 1.12 mm/s, $|\Delta E_Q|$ = 3.30 mm/s (solid blue trace); (ii) δ = 0.46 mm/s, $|\Delta E_Q|$ = 0.94 mm/s (solid trace); (iii) δ = 0.45 mm/s, $|\Delta E_Q|$ = 0.54 mm/s (dashed orange trace); (iv) δ =1.00 mm/s, $|\Delta E_Q|$ = 2.60 mm/s solid green trace). Residuals are shown in grey (SSE = 1.75 for C).

Simulation details for [LFe$_3$(F$_2$ArPz)$_2$(OFArPz)OFe][OTf] (6): The Mössbauer spectrum of **6** exhibits five well-resolved resonances, and bears close resemblance to the spectrum of **3**, demonstrating that the distal fluorine substitution has little impact on the local electronic structure about the Fe atoms. As with **3**, an asymmetric feature around 3 mm s^{-1} results from two nearly overlapping quadrupole doublets attributable to high spin ferrous ions, which, after simulation, results in a residual signal with four Lorentzians of nearly equal areas. As with **3**, of the two reasonable simulations (Fig. S41A–B), the one shown in Figure S41B provides a superior fit to the data, and also reveals Mössbauer parameters typical of high spin Fe(III) centers. Moreover, the observed isomer shifts agree well with those found for the Fe(III) centers of **3** (vide supra). Thus the simulation shown in Figure S41B is preferred to that shown in A.

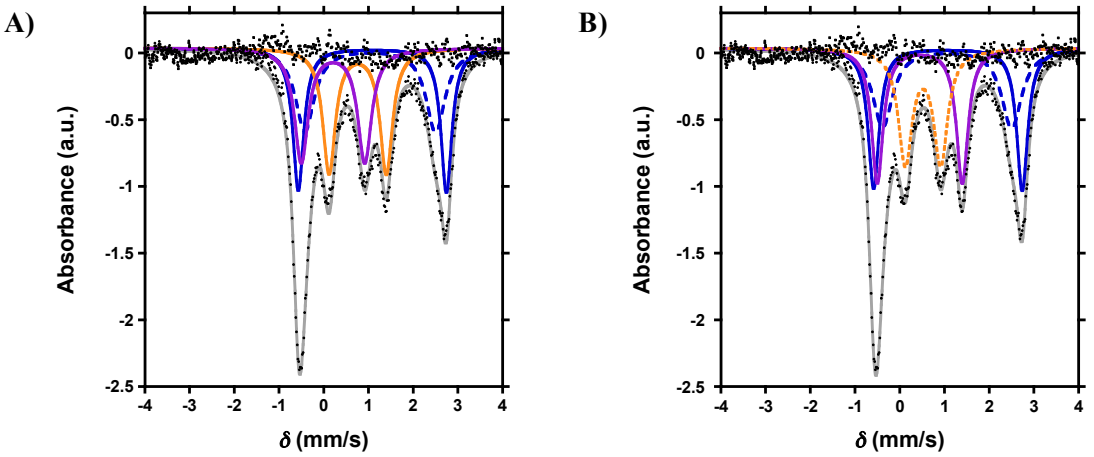

Figure S41. (A) Simulation of **6** (black dots) with four quadrupole doublets. Simulation is shown in grey, with parameters: (i) δ = 1.09 mm/s, $|\Delta E_Q|$ = 3.31 mm/s (solid blue trace); (ii) δ = 1.04 mm/s, $|\Delta E_Q|$ = 2.92 mm/s (dashed blue trace); (iii) δ = 0.76 mm/s, $|\Delta E_Q|$ = 1.28 mm/s (solid orange trace); and (iv) δ = 0.21 mm/s, $|\Delta E_Q|$ = 1.42 mm/s (solid purple trace). Residuals shown in black (SSE = 1.58). (B) Simulation of **6** (black dots) with four quadrupole doublets. Simulation is shown in grey, with parameters: (i) δ = 1.08 mm/s, $|\Delta E_Q|$ = 3.32 mm/s (solid blue trace); (ii) δ = 1.06 mm/s, $|\Delta E_Q|$ = 2.88 mm/s (dashed blue trace); (iii) δ = 0.52 mm/s, $|\Delta E_Q|$ = 0.80 mm/s (solid orange trace); and (iv) δ = 0.45 mm/s, $|\Delta E_Q|$ = 1.90 mm/s (solid purple trace); Residuals are shown in grey (SSE = 1.58 for A and SSE = 1.47 for B).

Simulation details for $[LFe_3(F_2ArPz)_2(OFArPz)OFe][OTf]_2$ (7): The Mössbauer spectrum of **7** exhibits only five well-resolved resonances. A single symmetric Lorentzian appearing around 3 mm s^{-1} suggests a single high spin ferrous center, while the residual signal is centered on 0.5 mm s^{-1}, within the range expected for high spin ferric ions. As with the spectrum of **2**, an initial simulation was performed using only three quadrupole doublets to fit the five observed features (Fig. S42A). After optimization, the refined parameters were consistent with two high spin Fe(III) and one high spin Fe(II) in a 2:1:1 ratio. Thus, to obtain a final simulation, the most intense Fe(III) signal was split into two distinct resonances, and all species were refined with equal populations (Fig. S42B).

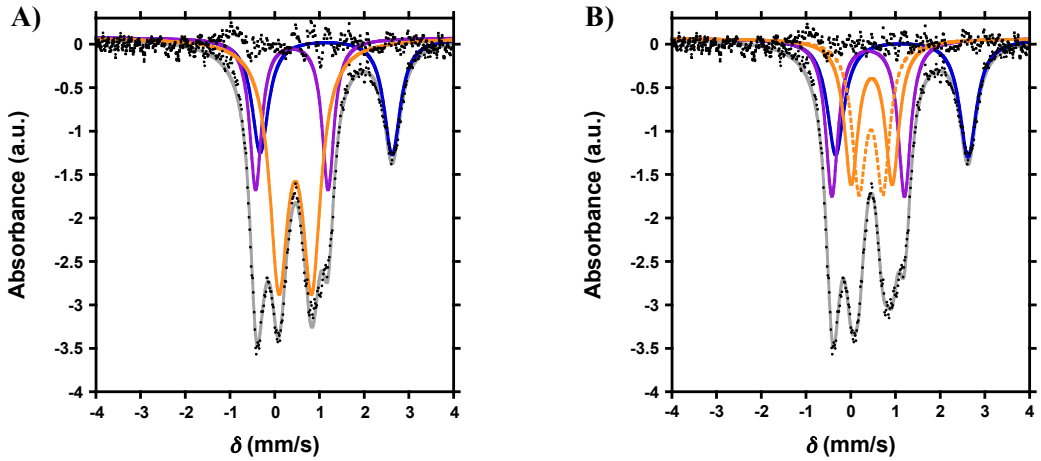

Figure S42. (A) Initial simulation of **7** (black dots) fit to three quadrupole doublets. Simulation is shown in grey, with parameters: (i) δ = 1.15 mm/s, $|\Delta E_Q|$ = 2.95 mm/s (26%, solid blue trace); (ii) δ = 0.46 mm/s, $|\Delta E_Q|$ = 0.74 mm/s (58%, solid orange trace); and (iii) δ = 0.39 mm/s, $|\Delta E_Q|$ = 1.62 mm/s (25%, solid purple trace). Residuals shown in black (SSE = 3.51). (B) Final simulation of **7** (black dots) fit to four quadrupole doublets. Simulation is shown in grey, with parameters: (i) δ = 1.15 mm/s, $|\Delta E_Q|$ = 2.96 mm/s (solid blue trace); (ii) δ = 0.47 mm/s, $|\Delta E_Q|$ = 0.92 mm/s (solid orange trace); (iii) δ = 0.45 mm/s, $|\Delta E_Q|$ = 0.54 mm/s (dashed orange trace); and (iv) δ = 0.39 mm/s, $|\Delta E_Q|$ = 1.62 mm/s (solid purple trace);. Residuals shown in grey (SSE = 2.73).

Simulation details for $[LFe_3(F_2ArPz)_3Fe(F)][OTf]_2$ (8): The Mössbauer spectrum of **8** resembles closely those observed for both **2** and **7**. A preliminary simulation with only three quadrupole doublets yields parameters consistent with two high spin Fe(III) and one high spin Fe(II) in a 2:1:1 ratio (Fig. S43A). Thus, to obtain a final simulation, the most intense Fe(III) signal was split into two distinct resonances, and all species were refined with equal populations (Fig. S43B).

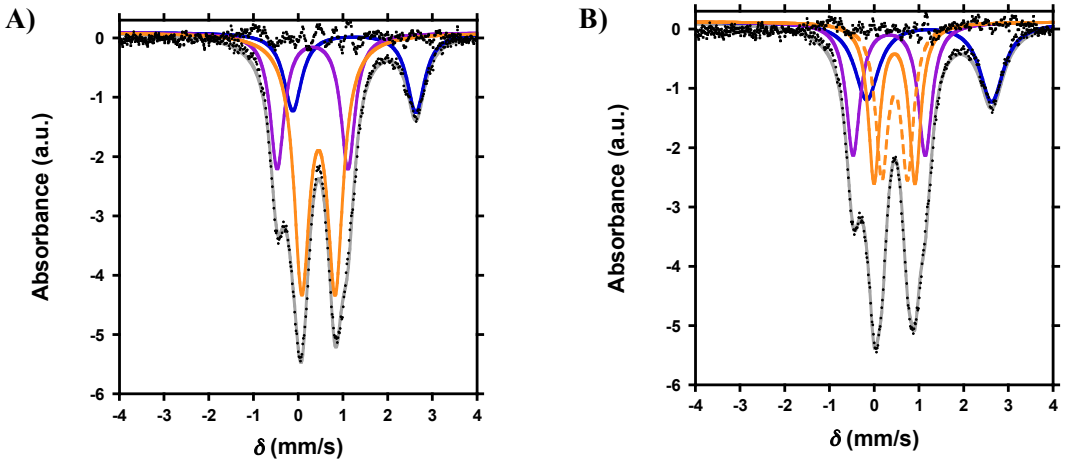

Figure S43. (A) Initial simulation of **8** (black dots) fit to three quadrupole doublets. Simulation is shown in grey, with parameters: (i) δ = 1.26 mm/s, $|\Delta E_Q|$ = 2.75 mm/s (21%, solid blue trace); (ii) δ = 0.46 mm/s, $|\Delta E_Q|$ = 0.75 mm/s (59%, solid orange trace); and (iii) δ = 0.32 mm/s, $|\Delta E_Q|$ = 1.58 mm/s (29%, solid purple trace. Residuals shown in black (SSE = 4.10). (B) Final simulation of **8** (black dots) fit to four quadrupole doublets. Simulation is shown in grey, with parameters: (i) δ = 1.23 mm/s, $|\Delta E_Q|$ = 2.79 mm/s (solid blue trace); (ii) δ = 0.46 mm/s, $|\Delta E_Q|$ = 0.92 mm/s (solid orange trace); (iii) δ = 0.46 mm/s, $|\Delta E_Q|$ = 0.58 mm/s (dashed orange trace); and (iv) δ = 0.34 mm/s, $|\Delta E_Q|$ = 1.61 mm/s (solid purple trace);. Residuals shown in grey (SSE = 4.16 for B).

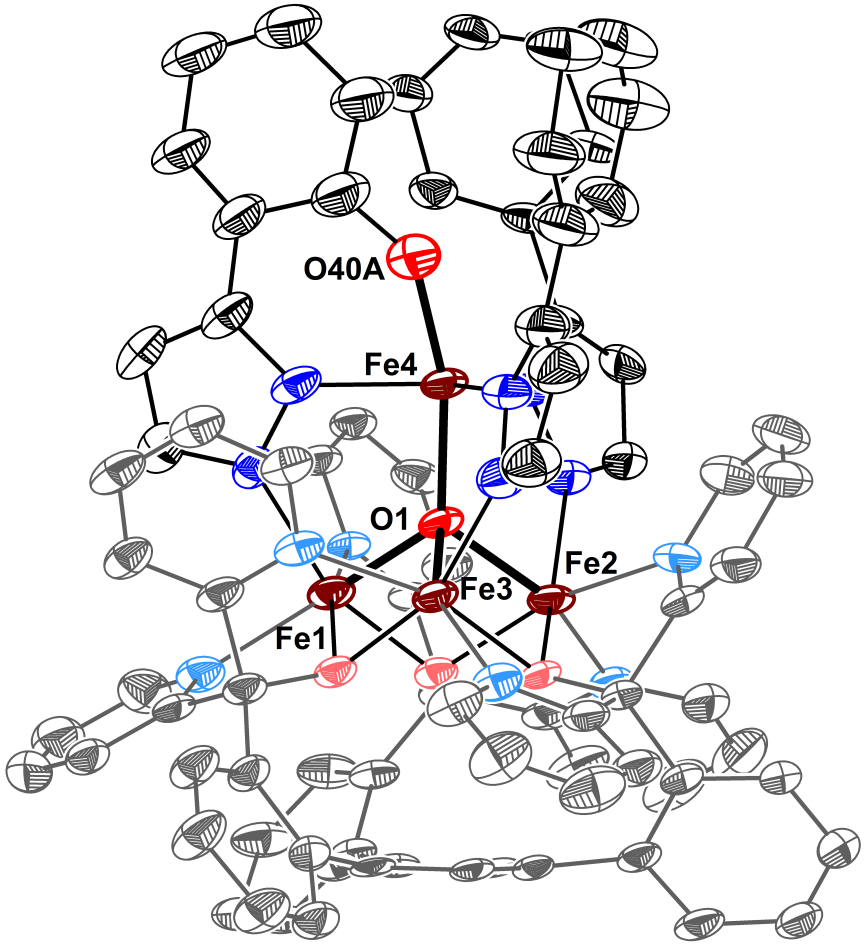

Figure S44. Crystal structure of $[LFe_3(PhPz)_3(OArPz)OFe][OTf]_2$ (**2**). Ellipsoids are shown at the 50% probability level. Hydrogen atoms, co-crystallized solvents molecules and outer sphere counter ions are not shown for clarity.

Special Refinement Details for $[LFe_3(PhPz)_2(OArPz)OFe][OTf]_2$. Compound **2** crystallizes in the monoclinic space group *C*2*c* with one molecule in the asymmetric unit together with two triflate counter ions and 1.3 molecules of co-crystallized diethyl ether, and 2.7 molecules of co-crystallized acetonitrile. Each of the pyrazolate bridging ligands was modeled as a mixture of 2-(1-pyrazol-3-yl)phenolate and 3-phenylpyrazolate. One of the triflate anions was disordered over two positions. One of the co-crystallized diethyl ether molecules is located near a crystallographic two-fold rotation axis. Additionally, there are two solvent accessible voids. One of which was modeled as a mixture of acetonitrile and diethyl ether. The other void was modeled as 2.5 molecules of acetonitrile disordered over five crystallographically independent positions. All of the diethyl ether molecules were modeled with the help of distance restraints on the 1,2-distances (C-C, 1.54(1); O-C 1.43(1)) and 1,3-distances (O-C, 2.43(2); C-C, 2.34(2).

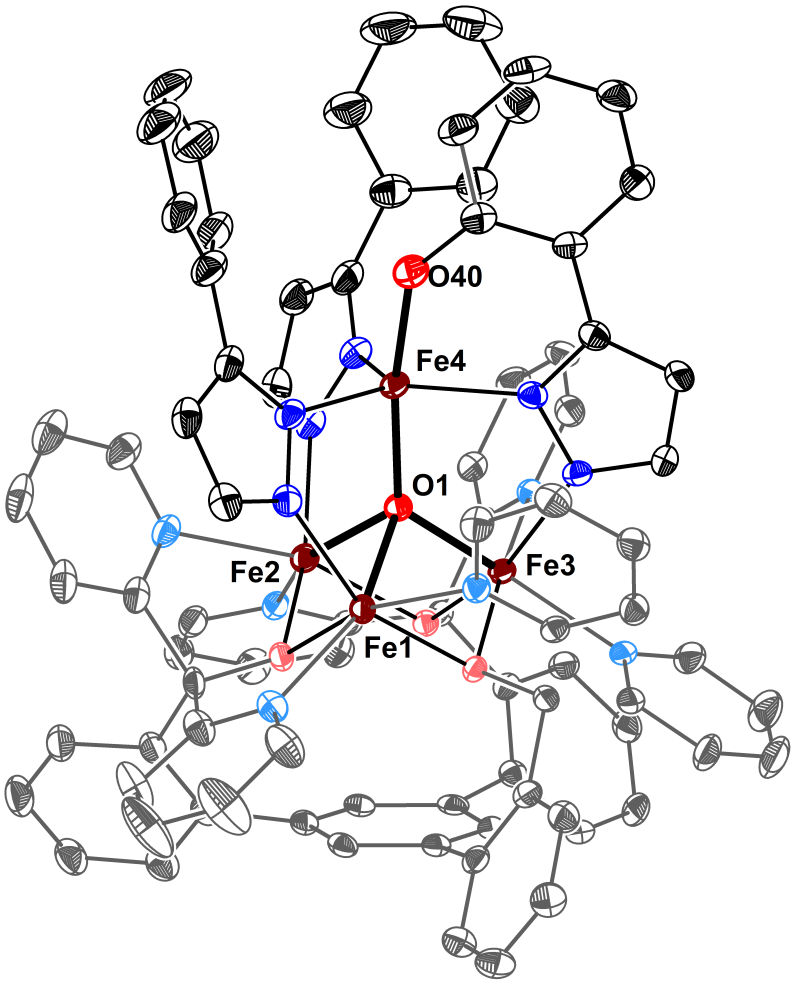

Figure S45. Crystal structure of [$LFe_3(PhPz)_2(OArPz)OFe$][OTf] (**3**). Ellipsoids are shown at the 50% probability level. Hydrogen atoms, co-crystallized solvents and outer sphere counter ions are not shown for clarity.

Special Refinement Details for [$LFe_3(PhPz)_2(OArPz)OFe$][OTf]. Compound **3** crystallizes in the monoclinic space group $P2_1/c$ with one molecule in the asymmetric unit along with a single triflate counter ion, two molecules of co-crystallized diethyl ether and two molecules of co-crystallized dichloromethane. One of the co-crystallized dichloromethane molecules has a rotational disorder and refined to occupancies of 36% and 64% respectively. The distances of both diethyl ether molecules were restrained 1.517 Å (C100–C101, C102–C103, C104–C105, and C106–C107), 1.411 Å (C101–O100, C102–O100, C105–O101, and C106–O101), 2.376 Å (C100–O100, C103–O100, C104–O101, and C107–O101), 2.743 Å (C101–C102 and C105–C106), and 4.743 Å (C100–C103 and C104–C107).

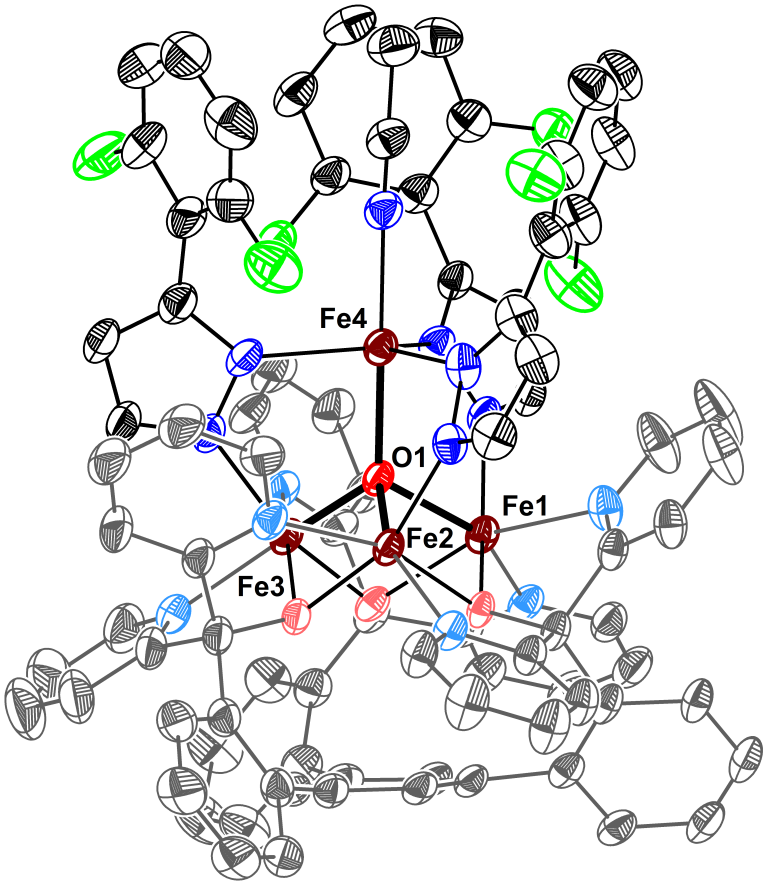

Figure S46. Crystal structure of $[LFe_3(F_2ArPz)_3OFe][OTf]_2$ (**5**). Ellipsoids are shown at the 50% probability level. Hydrogen atoms, co-crystallized solvents molecules and outer sphere counter ions are not shown for clarity.

Special Refinement Details for $[LFe_3(F_2ArPz)_3OFe][OTf]_2$. Compound **5** crystallizes in the monoclinic space group $P2_1/c$ with one molecule in the asymmetric unit along with two triflate counter ions, one molecule of co-crystallized diethyl ether and 2.8 molecules of co-crystallized acetonitrile. Both of the triflate counter ions were disordered over two positions. The co-crystallized diethyl ether and acetonitrile molecules are disordered over seven positions, two for diethyl ether and five for acetonitrile, in a large solvent accessible void. All acetonitrile molecules were refined with the help of distances restraints on the 1,2-distances (C-C, 1.16(1) and C-N, 1.54(1)) and 1,3-distances (C-C 2.75(1)).

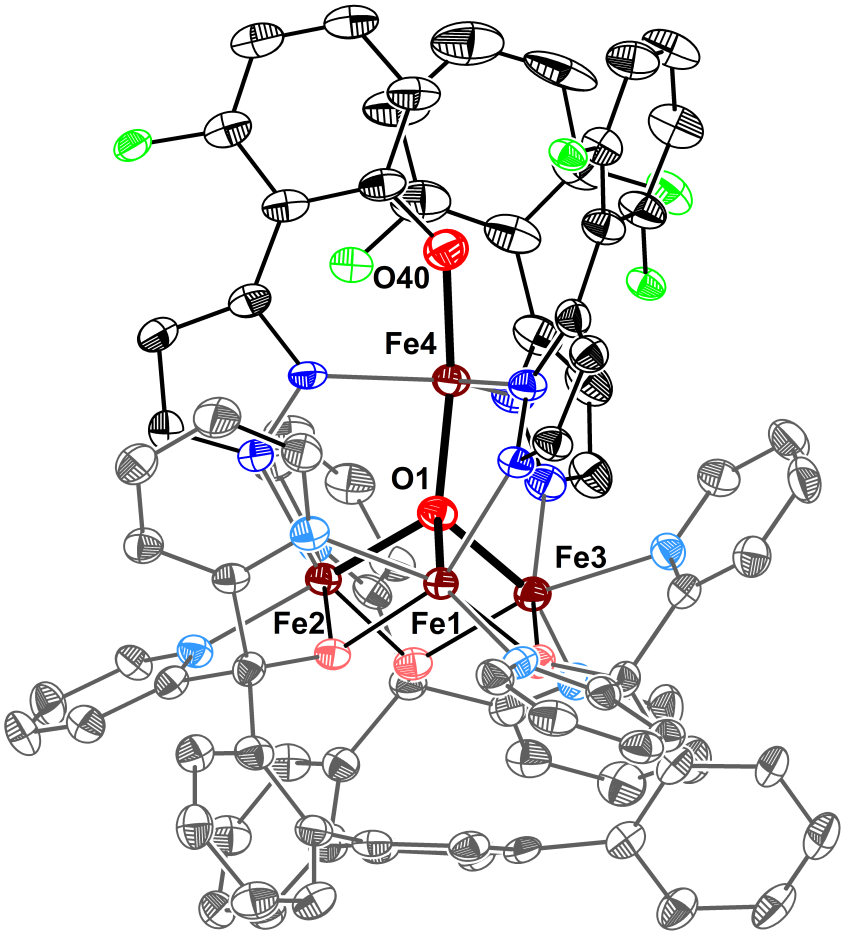

Figure S47. Crystal structure of $[LFe_3(F_2ArPz)_2(OFArPz)OFe][OTf]_2$ (**7**). Ellipsoids are shown at the 50% probability level. Hydrogen atoms, co-crystallized solvents molecules and outer sphere counter ions are not shown for clarity.

Special Refinement Details for $[LFe_3(F_2ArPz)_2(OFArPz)OFe][OTf]_2$. Compound **7** crystallizes in the monoclinic space group $P2_1/n$ with one molecule in the asymmetric unit along with two triflate counter ions, one molecule of co-crystallized diethyl ether, one molecule of co-crystallized water and 1.6 molecules of co-crystallized acetonitrile. One diethyl ether is disordered over two positions, with an additional occupational disorder with one acetonitrile. The disorder was satisfactorily modeled, and refined to occupancies of 60 % diethyl ether (O200 through C207), 60% acetonitrile (N2 through C203), and 40% diethyl ether (O201 through C211). The distances in one of the diethyl ether molecules (O201 through C211) were restrained at 1.517 Å (C211–C210 and C209–C208), 1.411 Å (C210–O201 and C209–O201), 2.357 Å (C211–O201 and C208-O201), and 4.743 Å (C211–C208). All acetonitrile molecules were refined with the help of distances restraints on the 1,2-distances (C-C, 1.458 and C-N, 1.157) and 1,3-distances (C-C 2.17). Enhanced rigid bond restraints were used on all solvent molecules.

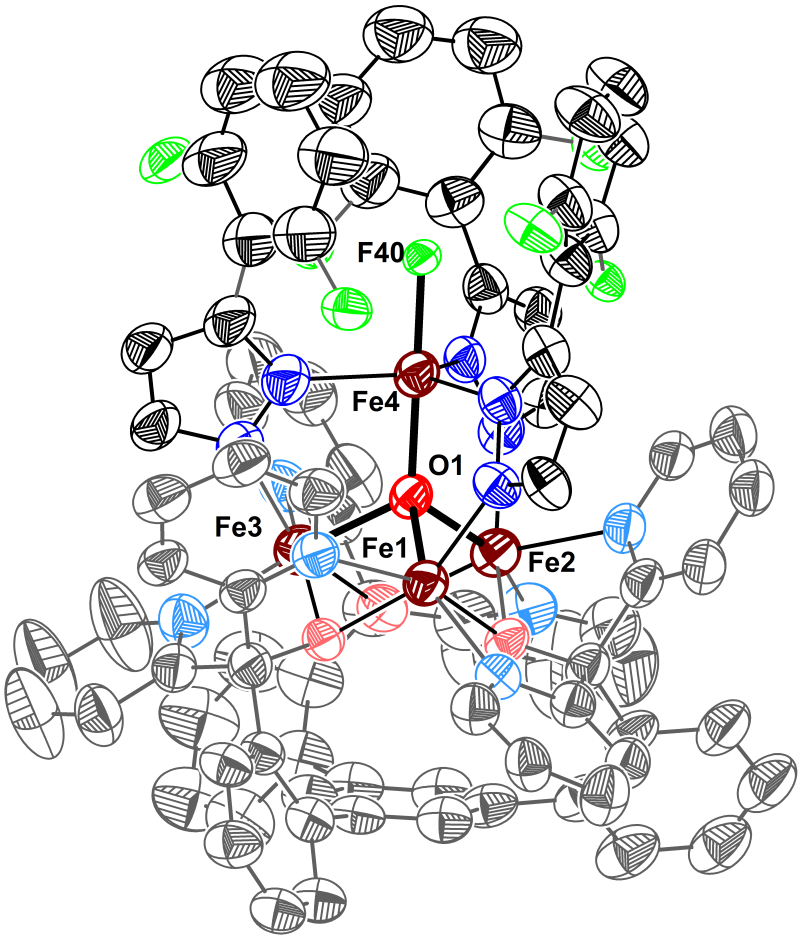

Figure S48. Crystal structure of $[LFe_3(F_2ArPz)_3OFe(F)][OTf]_2$ (**8**). Ellipsoids are shown at the 50% probability level. Hydrogen atoms, co-crystallized solvents molecules and outer sphere counter ions are not shown for clarity.

Special Refinement Details for $[LFe_3(F_2ArPz)_3OFe(F)][OTf]_2$. Compound **8** crystallizes in the monoclinic space group $P2_1/c$ with one molecule in the asymmetric unit along with two triflate counter ions, and one molecule of co-crystallized dichloromethane. Enhanced rigid bond restraints were used on the entire molecule. One of the triflates was disordered over two different positions refining to occupancies of 56% and 44% respectively. The co-crystallized dichloromethane molecule is disordered over five different positions and refined with occupancies of 8%, 10%, 10%, 25%, and 47%. All the disordered dichloromethane molecules are restrained to approximate isotropic behavior.

Table S1. Selected bond angles and distances for complexes **2**, **3**, and **5** and **7**.

Bond Distance (Å)	**Complex**			
	2[a]	**3**	**5**	**7**
Fe1–O1	2.054(4)	2.154(3)	2.154(3)	2.198(4)
Fe2–O1	2.076(4)	2.119(3)	1.941(3)	1.978(4)
Fe3–O1	1.999(4)	1.938(3)	1.919(3)	1.986(4)
Fe4–O1	1.931(4)	1.867(3)	2.042(3)	1.914(4)
Fe1–N13	2.090(5)	2.125(4)	2.116(4)	2.108(5)
Fe2–N23	2.068(5)	2.135(4)	2.074(4)	2.076(5)
Fe3–N33	2.064(3)	2.109(4)	2.095(4)	2.105(5)
Fe4–N14	2.065(4)	2.083(4)	2.083(4)	2.063(5)
Fe4–N24	2.049(5)	2.067(4)	2.113(4)	2.055(5)
Fe4–N34	2.047(6)	2.066(4)	2.131(4)	2.071(5)
Fe4-N40	-	-	2.149(4)	-
N13–N14	1.373(7)	1.375(5)	1.387(5)	1.365(7)
N23–N24	1.392(7)	1.404(6)	1.422(6)	1.374(7)
N33–N34	1.381(7)	1.381(5)	1.404(6)	1.367(7)
Fe4–O40	1.908(16)	1.911(3)	-	1.867(5)
Bond Angles (°)				
N14–Fe4–N24	121.4(2)	155.52(16)	117.22(15)	120.3(2)
N24–Fe4–N34	120.5(2)	113.85(15)	124.21(16)	117.5(2)
N34–Fe4–N14	117.8(2)	130.31(15)	117.30(16)	121.9(2)
O1–Fe4–O40	156.8(12)	163.68(14)	-	-
O1–Fe4–N40	-	-	175.46(15)	171.4(2)

[a]Bond angles and distances are taken from with the disordered part of **2** with a chemical occupancy of 49.1%.

Table S2. Crystal and refinement data for complexes **2**, **3**, and **5**.

	Complex **2**	Complex **3**	Complex **5**
CCDC	1432377	1432376	1432378
Empirical formula	$C_{96.5}H_{80.05}F_6Fe_4N_{14.7}O_{12.34}S_2$	$C_{95}H_{83}Cl_4F_3Fe_4N_{12}O_{10}S$	$C_{97.52}H_{75.28}F_{12}Fe_4N_{15.76}O_{11}S_2$
Formula weight (g/mol)	2044.49	2006.99	2159.38
T (K)	100	100	100
Radiation	MoKα (λ = 0.71073)	MoKα (λ = 0.71073)	MoKα (λ = 0.71073)
a (Å)	24.3192(13)	17.2200(5)	22.6768(14)
b (Å)	30.6264(16)	26.3779(9)	17.6060(11)
c (Å)	24.9005(14)	19.6922(6)	24.2443(14)
α (deg)	90	90	90
β (deg)	65.8456(17)	99.7240(10)	96.7988(18)
γ (deg)	90	90	90
V (Å^3)	9224.85(17)	8816.2(5)	9611.4(10)
Z	4	4	4
Cryst. syst.	Monoclinic	Monoclinic	Monoclinic
Space group	C2/c	$P2_1/c$	$P2_1/c$
ρ_{calc}g (cm^3)	1.472	1.512	1.492
2 σ range (deg)	4.46 to 50.046	4.47 to 53.468	3.28 to 54.984
Crystal size/mm	0.20 × 0.19 × 0.09	0.22 × 0.19 × 0.10	0.35 × 028 × 0.26
μ (mm^{-1})	0.745	0.865	0.727
GOF	1.042	1.046	1.053
R1, wR2 (I> 2σ (I))	R_1 = 0.0773, wR_2 0.2051	R_1 = 0.0683, wR_2 0.1774	R_1 = 0.0792, wR_2 0.2235

Table S3. Crystal and refinement data for complexes **7** and **8**.

	Complex **7**	Complex **8**
CCDC	1432375	-
Empirical formula	$C_{93.2}H_{70.8}F_{11}Fe_4N_{13.6}O_{13}S_2$	$C_{87}H_{53}Cl_2F_{13}Fe_4N_{12}O_{10}S_2$
Formula weight (g/mol)	2085.75	2031.83
T (K)	100	100
Radiation	CuKα (λ = 1.5478)	CuKα (λ = 1.5478)
a (Å)	14.9873(4)	22.4130(9)
b (Å)	26.9656(7)	16.4854(8)
c (Å)	22.7659(6)	24.6252(12)
α (deg)	90	90
β (deg)	100.818(2)	96.581(3)
γ (deg)	90	90
V (Å^3)	9037.1(4)	9038.7(7)
Z	4	4
Cryst. syst.	Monoclinic	monoclinic
Space group	$P2_1/n$	$P2_1/c$
ρ_{calc}g (cm^3)	1.533	1.493
2 σ range (deg)	5.134 to 149.08	3.968 to 141.102
Crystal size/mm	0.15 × 0.1 × 0.04	0.2 × 0.1 × 0.1
μ (mm^{-1})	6.292	6.809
GOF	1.012	1.151
R1, wR2 (I> 2σ (I))	R_1 = 0.0857, wR_2 = 0.2060	R_1 = 0.1492, wR_2 = 0.3675

Table S4. Mössbauer parameters for complexes **2,3, and 5-8**

#	Complex	Parameters			
		δ (mm/s)	**$\lvert \Delta E_q \rvert$ (mm/s)**	**Γ (mm s^{-1})**	**Relative area**
2	$[LFe_3(PhPz)_2(OArPz)OFe][OTf]_2$	0.47	0.99	0.39	0.26
		0.47	0.56	0.39	0.26
		1.17	2.96	0.52	0.26
		0.40	1.72	0.40	0.26
3	$[LFe_3(PhPz)_2(OArPz)OFe][OTf]$	0.52	0.77	0.40	0.27
		1.07	3.25	0.30	0.27
		1.09	2.89	0.59	0.27
		0.46	1.84	0.31	0.27
5	$[LFe_3(F_2ArPz)_3OFe][OTf]_2$	0.46	0.94	0.36	0.27
		0.45	0.54	0.37	0.27
		1.12	3.30	0.40	0.27
		1.00	2.60	0.53	0.27
6	$[LFe_3(F_2ArPz)_2(OFArPz)OFe][OTf]$	0.52	0.80	0.38	0.27
		1.08	3.32	0.30	0.27
		1.06	2.88	0.55	0.27
		0.45	1.90	0.31	0.27
7	$LFe_3(F_2ArPz)_2(OFArPz)OFe][OTf]_2$	0.47	0.92	0.38	0.27
		0.45	0.54	0.37	0.27
		1.15	2.96	0.46	0.27
		0.39	1.62	0.34	0.27
8	$[LFe_3(F_2ArPz)_3OFe(F)][OTf]_2$	0.46	0.92	0.31	0.28
		0.46	0.58	0.33	0.28
		1.23	2.79	0.65	0.28
		0.34	1.61	0.37	0.28

References.

1) Huang, C.-Y.; Doyle, A. G. *J. Am. Chem. Soc.* **2012**, *134*, 9541.
2) de Ruiter G.; Thompson, N. B.; Lionetti, D.; Agapie, T. *J. Am. Chem. Soc.* **2015***, 137,* 14094.
3) Yoshida, I.; Yoneda, N.; Ohashi, Y.; Miyamoto, M.; Miyazaki, F.; Seshimo, H.; Kamata, J.; Takase, Y.; Shirato, M.; Shimokubo, D.; Sakuma, Y.; Yokohama, H.; Eisai Co., Ltd., **2004**; EP 1 382 603 A1, p 117.
4) Nagarathnam, D.; Vakkalanka, S. K. V. S.; Muthuppalaniappan, M.; Viswanadha, S.; Babu, G.; Bhavar, P. K.; Rhizen Pharmaceuticals SA. **2012**; US 2012/0289496 A1, p 100.
5) APEX-II *Version 2 User Manual, M86-E01078, Bruker Analytical X-ray Systems,* Madison, WI, June 2006.
6) Sheldrick, G. M. *"SADABS (version 2008/1): Program for Absorption Correction for Data from Area Detector Frames",* University of Göttingen, 2008.
7) Sheldrick, G. M. *Acta Crystallogr., Sect. A: Found. Crystallogr.* **2008**, *64*, 112.
8) Herbert, D. E.; Lionetti, D.; Rittle, J.; Agapie, T. *J. Am. Chem. Soc.* **2013**, *135*, 19075.
9) Gouré, E.; Carboni, M.; Dubourdeaux, P.; Clémancey, M.; Balasubramanian, R.; Lebrun, C.; Bayle, P.-A.; Maldivi, P.; Blondin, G.; Latour, J.-M. *Inorg. Chem.* **2014**, *53*, 10060.
10) Lalia-Kantouri, M.; Papadopoulos, Christos D.; Hatzidimitriou, Antonios G.; Bakas, T.; Pachini, S. *Z. Anorg. Allg. Chem.* **2010**, *636*, 531.
11) Singh, A. K.; Jacob, W.; Boudalis, A. K.; Tuchagues, J.-P.; Mukherjee, R. *Eur. J. Inorg. Chem.* **2008**, *2008*, 2820.
12) Chardon-Noblat, S.; Horner, O.; Chabut, B.; Avenier, F.; Debaecker, N.; Jones, P.; Pécaut, J.; Dubois, L.; Jeandey, C.; Oddou, J.-L.; Deronzier, A.; Latour, J.-M. *Inorg. Chem.* **2004**, *43*, 1638.
13) Schmitt, W.; Anson, C. E.; Pilawa, B.; Powell, A. K. *Z. Anorg. Allg. Chem.* **2002**, *628*, 2443.
14) Reynolds, R. A.; Coucouvanis, D. *Inorg. Chem.* **1998**, *37*, 170.
15) Murali, M.; Nayak, S.; Costa, J. S.; Ribas, J.; Mutikainen, I.; Turpeinen, U.; Clémancey, M.; Garcia-Serres, R.; Latour, J.-M.; Gamez, P.; Blondin, G.; Reedijk, J. *Inorg. Chem.* **2010**, *49*, 2427.
16) Sutradhar, M.; Carrella, L. M.; Rentschler, E. *Eur. J. Inorg. Chem.* **2012**, *2012*, 4273.